EV WIRELESS CHARGER

An Undergraduate Research Scholars Thesis

by

ALYSSA BROWN AND TEDDY LEHMAN

Submitted to the LAUNCH: Undergraduate Research office at
Texas A&M University
in partial fulfillment of the requirements for the designation as an

UNDERGRADUATE RESEARCH SCHOLAR

Approved by
Faculty Research Advisor: Dr. Oscar Moreira

May 2022

Major: Electrical Engineering

RESEARCH COMPLIANCE CERTIFICATION

Research activities involving the use of human subjects, vertebrate animals, and/or biohazards must be reviewed and approved by the appropriate Texas A&M University regulatory research committee (i.e., IRB, IACUC, IBC) before the activity can commence. This requirement applies to activities conducted at Texas A&M and to activities conducted at non-Texas A&M facilities or institutions. In both cases, students are responsible for working with the relevant Texas A&M research compliance program to ensure and document that all Texas A&M compliance obligations are met before the study begins.

We, Alyssa Brown and Teddy Lehman, certify that all research compliance requirements related to this Undergraduate Research Scholars thesis have been addressed with my Research Faculty Advisor prior to the collection of any data used in this final thesis submission.

This project did not require approval from the Texas A&M University Research Compliance & Biosafety office.

TABLE OF CONTENTS

ABSTRACT

EV Wireless Charger

Alyssa Brown, Teddy Lehman
Department of Electrical and Computer Engineering
Texas A&M University

Research Faculty Advisor: Dr. Oscar Moreira
Department of Electrical and Computer Engineering
Texas A&M University

As electric vehicles of all sizes become more popular, the demands for convenient ways of powering them grow as well. Wireless chargers have become a preferred alternative to conventional wired chargers for their convenience and safety features. This thesis covers the design and testing of a wireless charger suitable for a small electric vehicle such as an E-bike. An inductive based power transfer is used along with key electronics including inverters, rectifiers, buck and boost converters. Another important element to this design is its ability to use either a DC or AC primary source. This makes the charger more versatile than single source designs by allowing for the choice of a power grid connection or an off-grid power such as through a solar panel. The design process for all components will be discussed and followed with simulation results showing ideal performance. A prototype is also constructed to provide real life analysis of the design and to determine effects of misalignment.

DEDICATION

To our families, instructors, peers, and especially our mascot, Tiny Dancer, who supported us throughout the research process.

ACKNOWLEDGMENTS

Contributors

We would like to thank our faculty advisor, Dr. Oscar Moreira, and our senior design professor Dr. John Lusher as well as Dr. Prasad Enjeti for their guidance and support throughout the course of this research.

Thanks also go to our friends and colleagues and the department faculty and staff for making our time at Texas A&M University a great experience. Finally, thanks to Jimmy and Lily for their encouragement, patience and love.

The materials used for our EV Wireless Charger were in part provided by our ECEN Capstone Project Funding. Measurement tools used were provided by the Fischer Engineering Design Center at Texas A&M University.

All other work conducted for the thesis was completed by the students independently.

NOMENCLATURE

A	Amp
AC	Alternating Current
DC	Direct Current
EV	Electric Vehicle
F	Farad
H	Henry
IC	Integrated Circuit
IoT	Internet of Things
IPT	Inductive Power Transfer
Hz	Hertz
kHz	Kilohertz (1,000 Hz)
V	Volt
WPT	Wireless Power Transfer

1. INTRODUCTION

Current research on wireless power transfer (WPT) systems has a few major goals in mind. Among these goals are improving efficiency, increasing range, and creating dynamic designs [1] [2]. One primary motivation behind increased range is to power IoT devices, and research is being done to power these devices remotely [3]. In terms of electric vehicles, many researchers are looking into creating WPT systems that can be implemented into roadways thus allowing for dynamic charging as the vehicle drives. This is especially important for the future use of autonomous vehicles as a source of transportation [4]. As with all battery chargers, efficiency of the system is important. Over the years, there has been significant development of WPT systems to maximize efficiency such as improvement of the utilized control system [5]. Research into efficiency even extends to corner cases where new issues arise, such as underwater power transfer, where eddy current losses become non-negligible and special considerations must be made [6]. There has been limited research into the application of multiple power supplies, and how that might improve operability of the WPT systems, so pursuing that objective may lead to new improvements in the field.

1.1 Motivation

The upcoming widespread use of electrical vehicles is sparking innovation in ways to efficiently transfer power to these vehicles beyond wired charging. Wireless power transfer is becoming a method of interest due to its better safety ratings and ease of use. As renewable energy becomes more accessible, the DC power that comes from solar panels enters the hands of consumers. Creating wireless chargers that can directly harness the renewable energy, while having the option to fall back on the more stable power grid, could mean increased efficiency and cost savings, all while maintaining the reliability that comes with the electric grid. While stability at the source is important, it is also essential for a charger to have stability at the input of the battery in order to have controlled and efficient charging. One potential avenue for this improvement is

the implementation of a boost converter on the secondary side to regulate coil output. Thus, we endeavored to design and build a WPT system that adopts these methods which will be tested.

1.2 Organization

This work is organized in four main chapters after the introduction. Chapter two provides background on the theory and circuitry used in the design of the wireless charger. This discussion is followed by the design steps taken in both calculation and simulation to ensure a valid system. The Results chapter covers the data collected from simulations as well as the hard data gathered from the constructed prototype. Finally, any findings or revelations are discussed in the conclusion chapter which is followed by the list of references used throughout the work.

2. BACKGROUND

This chapter describes the basic principles of wireless power transfer as well the the functionality of the power electronics used in the charger's design. It begins with an overview of the theory behind wireless power transfer. Following this is an overview of rectifier and inverter operation as well as a detailed description of the boost and buck converter topologies used in this design.

2.1 Wireless Power Transfer Theory

The type of wireless power transfer used in this work is inductive coupling based. This involves two coils, one called the primary coil which has a source attached to it and another called the secondary coil which receives the wireless transferred power. An AC voltage source can be applied to the primary coil whose current will create a magnetic field in the core of the coil. When the coils are aligned with one another, as demonstrated in figure 2.1, the magnetic field produced by the primary coil will induce a current/voltage in the secondary coil, delivering power without wires.

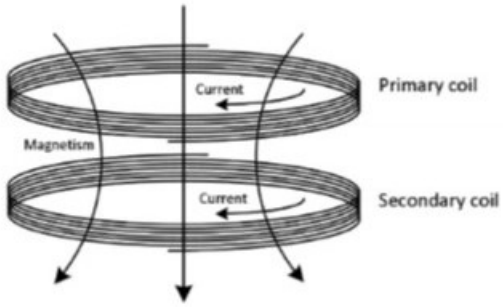

Figure 2.1: Inductive Coupling Diagram [7]

In calculations and simulations, these two coils can be modeled as an inductive transformer and follow a similar ideal behavior. An ideal transformer has no internal resistance and a maximum coupling coefficient k = 1. Thus the mutual inductance between the primary (L_1) and secondary (L_2) coil is at a maximum and is given by

$$M = \sqrt{L_1 L_2}. \tag{2.1.1}$$

The inductance of the coils is proportional to the square of the number of turns it has been wound. Let N_1 be the turns of the primary coil and N_2 be the number of turns for the secondary coil. A ratio can be formed called the turns ratio (n) which can also be describes as the gain of the transformer. This ratio is given below

$$n^2 = \frac{L_2}{L_1} = \frac{N_2^2}{N_1^2} \tag{2.1.2}$$

Using the circuit model for an ideal transformer with dots on the same end for the coils, as shown in figure, we can further derive that the ratio of the primary ($\mathbf{V_1}$) and secondary ($\mathbf{V_2}$) voltages is the turns ratio.

$$\begin{aligned}
\mathbf{V_1} &= j\omega L_1 \mathbf{I_1} - j\omega M \mathbf{I_2} \\
&= j\omega L_1 \mathbf{I_1} - j\omega \sqrt{L_1 L_2} \mathbf{I_2} \\
&= j\omega L_1 \mathbf{I_1} - j\omega L_1 n \mathbf{I_2} \\
\mathbf{V_1} &= j\omega L_1 (\mathbf{I_1} - n\mathbf{I_2})
\end{aligned} \tag{2.1.3}$$

Following a similar approach, the equation for $\mathbf{V_2}$ can be derived as

$$\mathbf{V_2} = j\omega L_2 \mathbf{I_2} - j\omega M \mathbf{I_1} = j\omega L_1 (\mathbf{I_1} - n\mathbf{I_2}) n \tag{2.1.4}$$

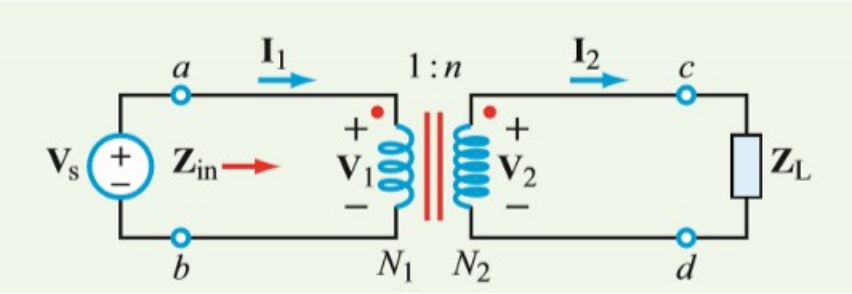

Figure 2.2: Ideal Transformer Circuit [8]

Dividing Eq. 2.1.4 by Eq. 1.3 we see that the turns ratio is also defined as the ratio of the secondary voltage to the primary voltage.

$$\frac{\mathbf{V_2}}{\mathbf{V_1}} = n \tag{2.1.5}$$

This fact is important in the design of a wireless charger as the turns ratio of the coils can be used to increase or decrease the voltage from the primary to the secondary to the necessary voltage level for charging.

2.2 Rectifier Theory

A rectifier operates on the ability of a diode to only conduct current in one direction. With just one diode, Current can be conducted during only the positive phase of the AC input, charging a capacitor which can provide the output current when the diode is off. Figure 2.3 shows this simple setup, and Figure 2.4 shows the result of using this architecture.

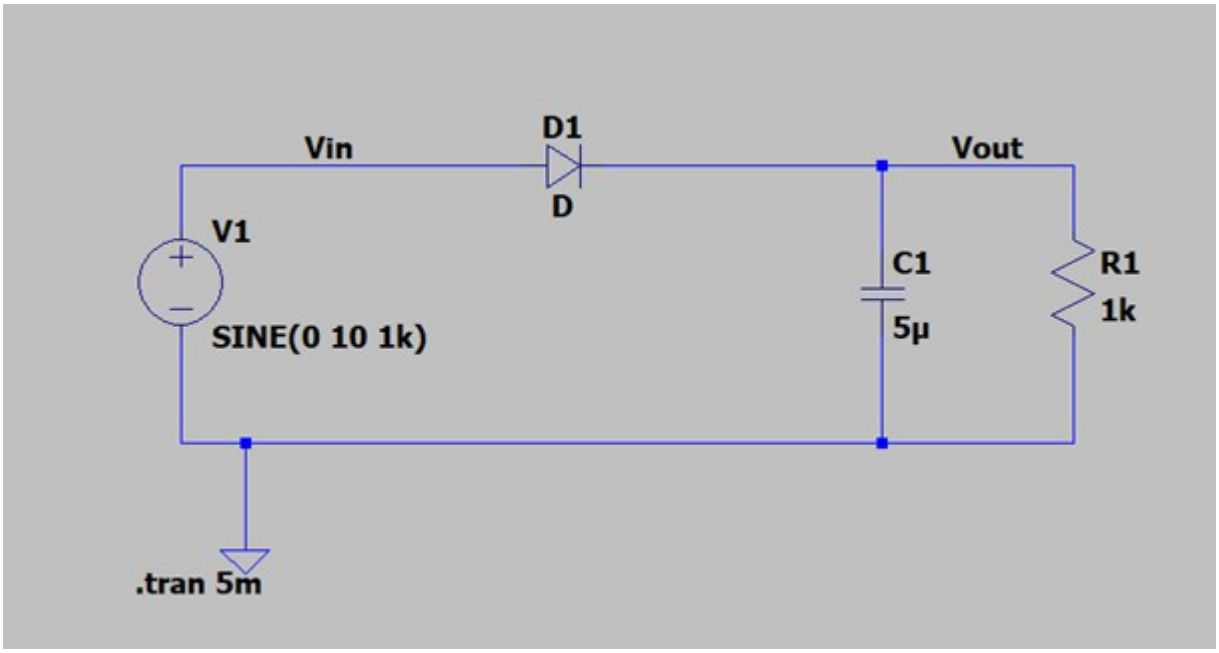

Figure 2.3: Simple Rectifier Output

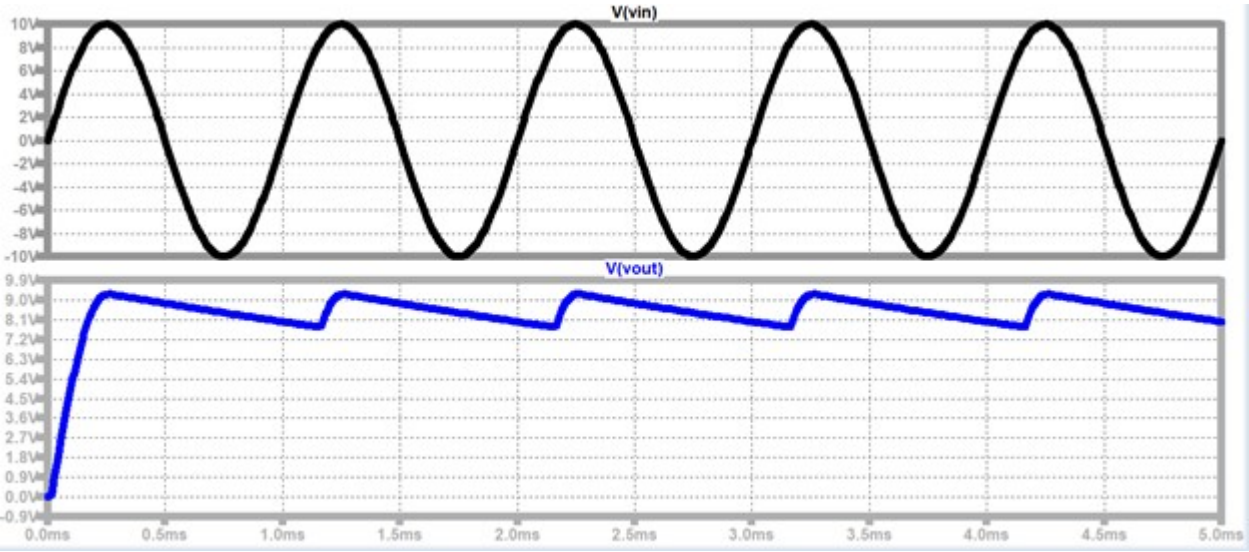

Figure 2.4: Simple Rectifier Circuit

This design only conducts from the source during the positive phase. To allow for charging during the positive and negative phases, two identical paths of diodes must be used. In Figure 2.5 below, D2 and D3 form the current path during the positive phase, allowing current to flow first from ground into the negative terminal, and then through the source to the positive terminal, which charges the capacitor through the diode until the source drops below the diodes threshold, stopping conduction. D1 and D4 perform the same when Vin+ is negative and Vin- is positive.

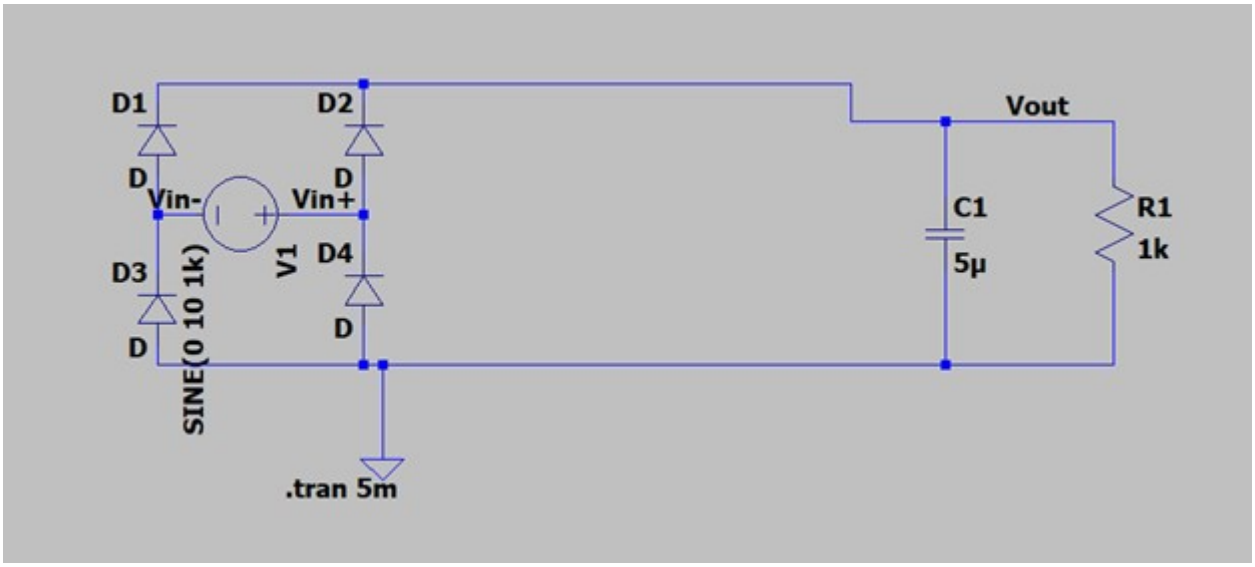

Figure 2.5: Full Bridge Rectifier Circuit

Figure 2.6 demonstrates the conducting phases more clearly, showing how D2 conducts while the input is positive, and D1 conducts when the input is negative. The load/capacitor views both of these phases identically, as can be seen from how the current is the same for both phases.

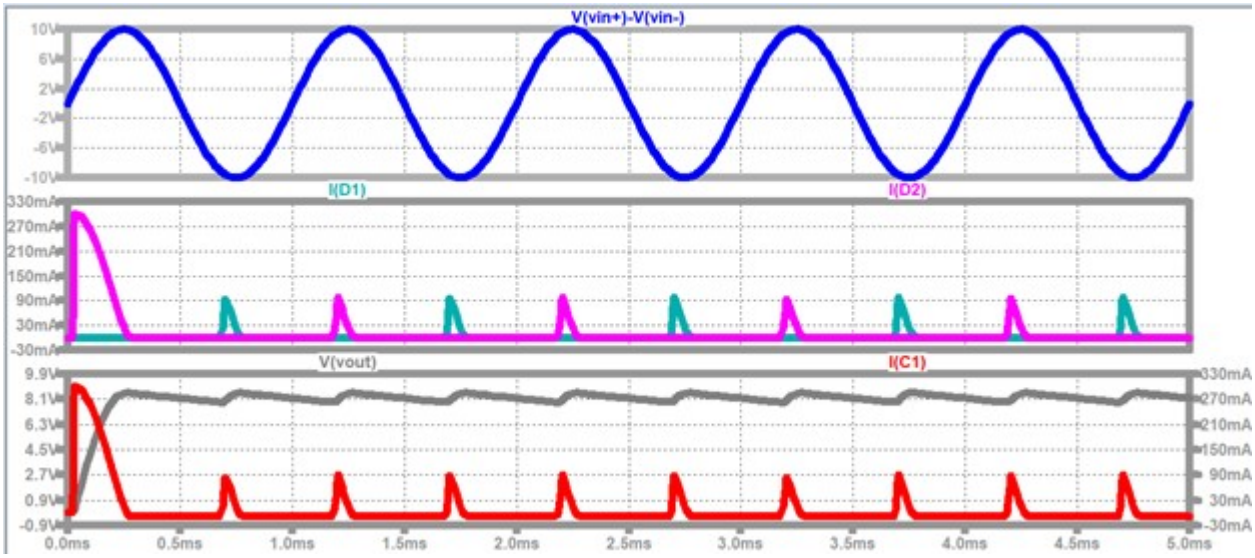

Figure 2.6: Full Bridge Rectifier Output

2.3 Inverter Theory

The inverter functions through four switches, which control the two nodes of the output. Each node is connected to two switches, one leading to the power supply, and the other to ground. When the top switch is activated, it will pull the output node up to the power supply, VDD, and when the bottom switch is activated, it will pull the node down to ground. By giving complimentary inputs to the switches on either end of the output, the differential output voltage will alternate between positive and negative, at the frequency of the switch control signals. It is important to ensure that two switches in a stack are not on at the same time, which would short the power supply to ground and potentially damage devices. Figure 2.7 shows how this can be realized, while Figure 2.8 shows the controls signals for the left branch of the inverter. The result can be seen in Figure 2.9, showing how one node switches from 20V to ground, and the differential output switches from +20V to -20V.

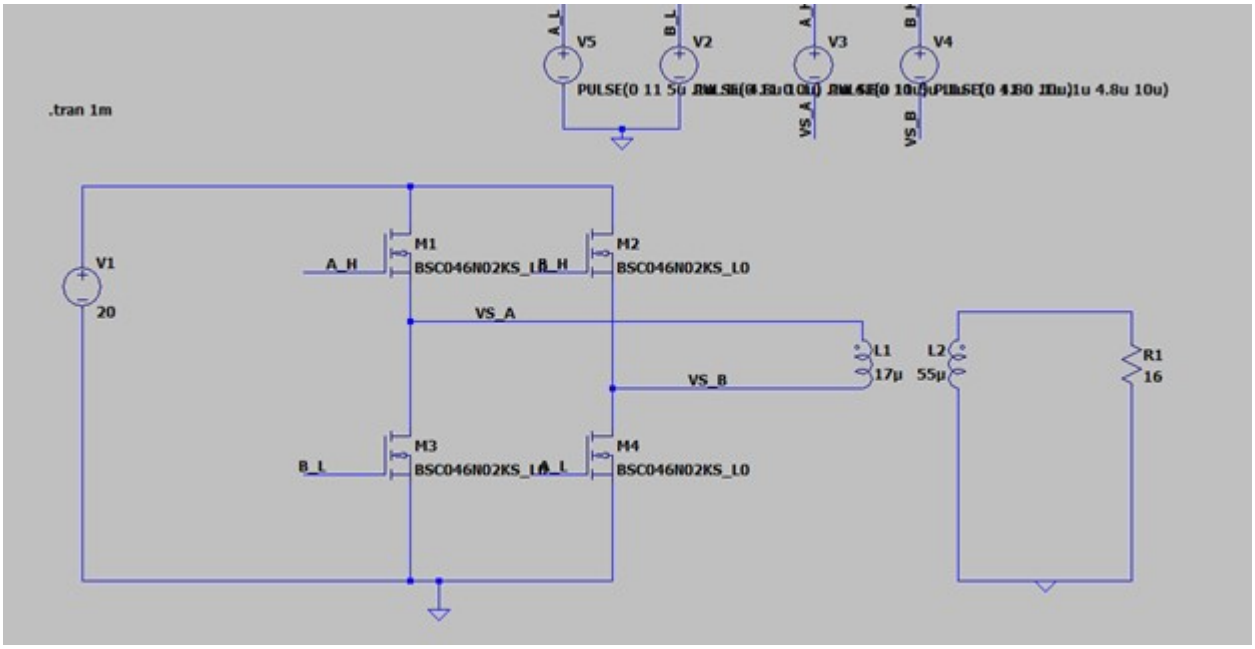

Figure 2.7: Inverter Circuit

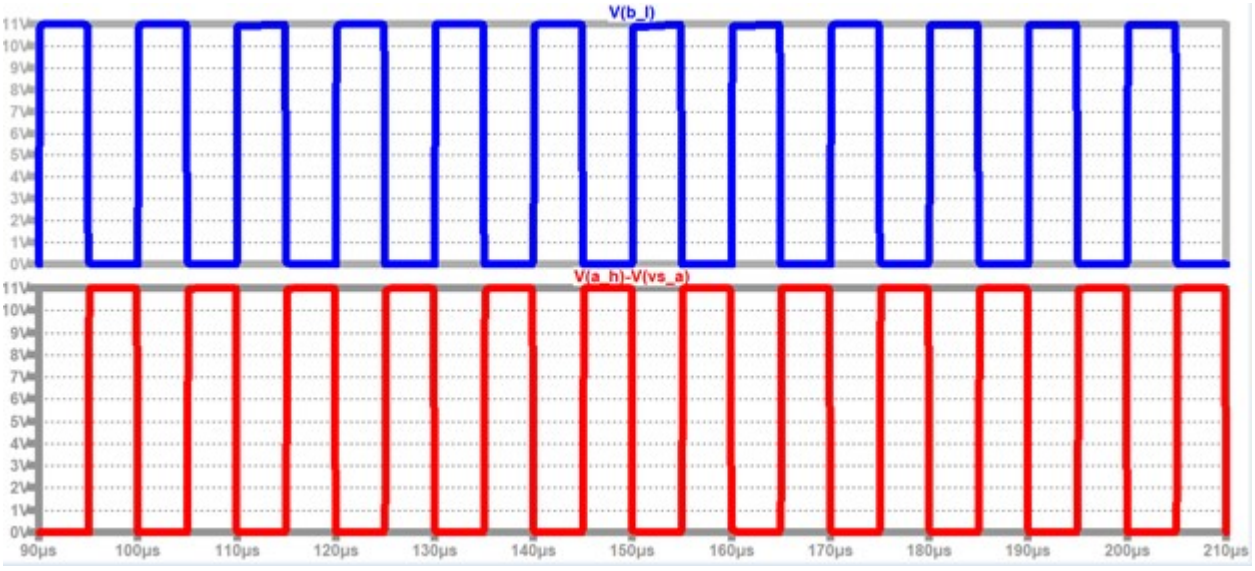

Figure 2.8: Inverter Switch Control Signals

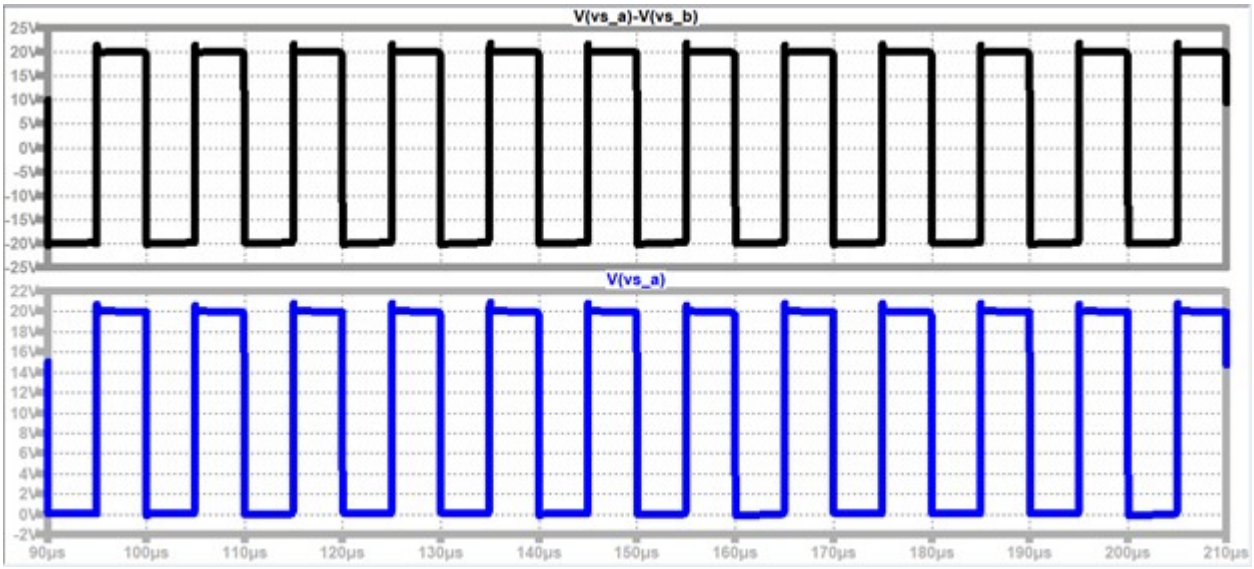

Figure 2.9: Inverter Output

2.4 Buck Converter Theory

A buck converter fundamentally operates by controlling the charging and discharging of an inductor and capacitor. By varying the duty cycle of a switch, the inductor can be charged more or less within a given period, which in turn charges and discharges a capacitor. When this inductor, capacitor, and a load are all in equilibrium, we can achieve a steady output voltage, which is approximately the supply voltage multiplied by the duty cycle of the switch. A diode is required to allow the inductor to continue conduction current when the switch is turned off. By varying the duty cycle, the output voltage can be controlled. The most common way to vary the duty cycle is through feedback.

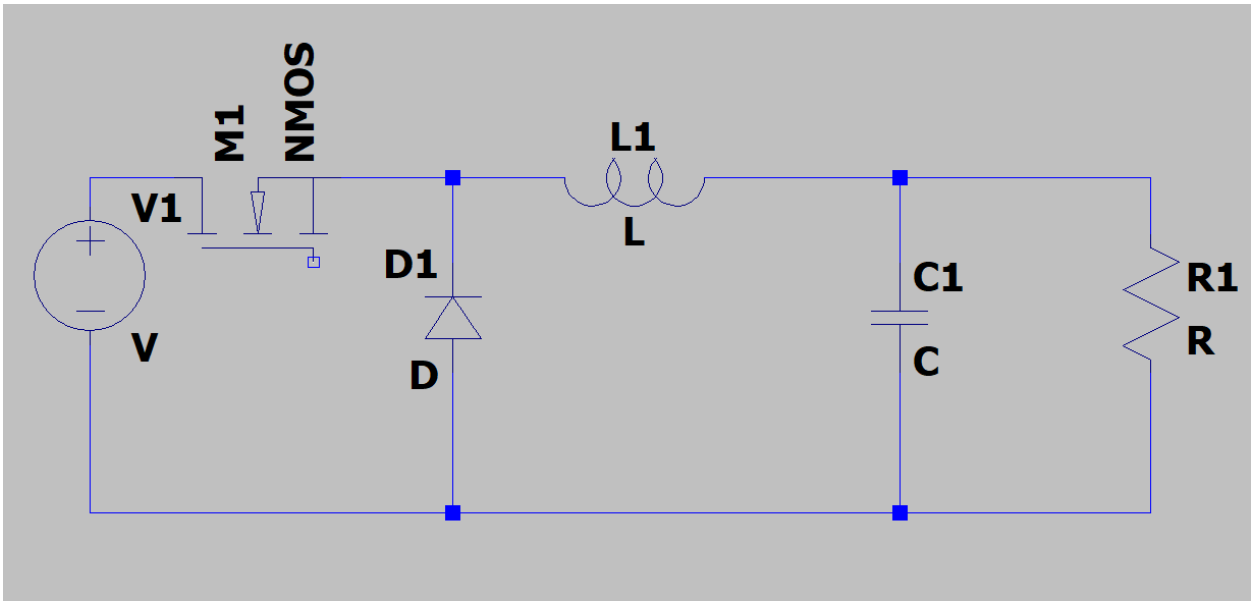

Figure 2.10: Simple Buck Converter

The buck converter can be better controlled through a feedback error amplifier. This error correcting amplifier compares the output voltage, or a proxy of it through a resistive voltage divider, to a reference voltage. Pulse width modulation is used to turn the output of the error amplifier into a series of signals to control the gate, for instance when the difference between the output voltage and the reference voltage is positive, the pulse width modulation might decrease the duty cycle of the switch, in turn reducing the output voltage until the error amplifier detects no difference.

2.5 Boost Converter Theory

A boost converter operates on similar fundamentals as a buck converter, wherein a switch controls the charging and discharging of an inductor, but instead of connecting the inductor to the input power, the switch instead connects the inductor to ground. This allows the inductor to charge with one terminal at the input source and the other terminal at ground, and then when the switch is turned off, the current flows to charge the output capacitor by passing through a diode.

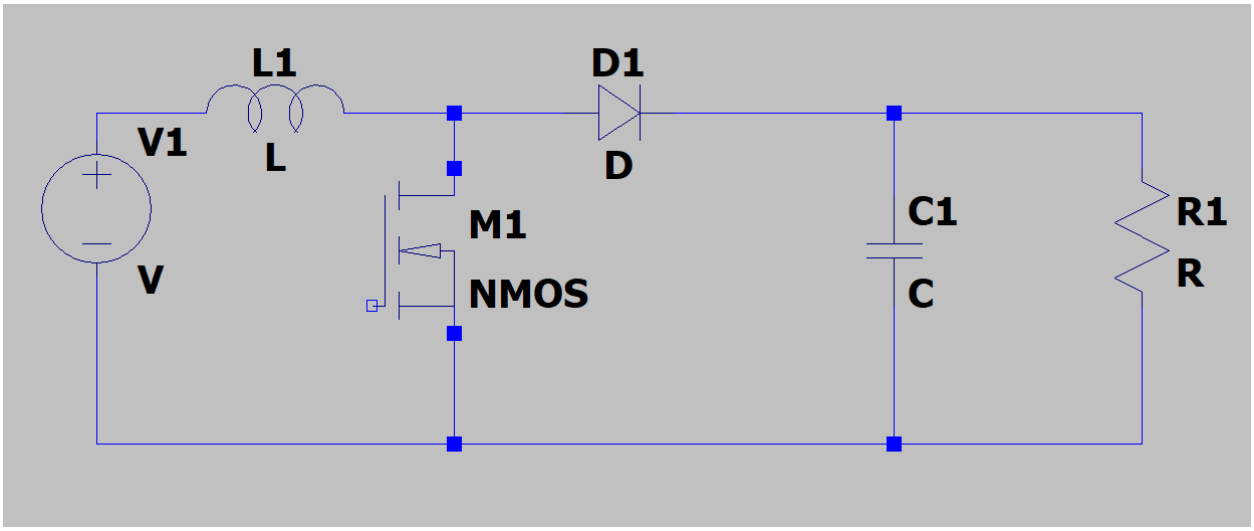

Figure 2.11: Simple Boost Converter

A similar feedback network can be implemented to control the output voltage against variations in the input.

3. DESIGN

In this chapter, the design methodology used for all components of the charger is discussed. We begin with the primary side electronics for driving the wireless power transfer, followed by the design of the coils use for power delivery and finally cover the secondary side electronics used for optimal charging of a battery.

3.1 Design of Primary Side Electronics

The primary side electronics include a transformer, a full-bridge rectifier, two buck converters, an inverter driver and a H-bridge inverter. These electronics provide the versatility of AC or DC power source as well as stepping down internal voltages for safe driving of the wireless power system. IC chips were utilized for maximum efficiency and sensible control. Below is a black box diagram for the subsystem design.

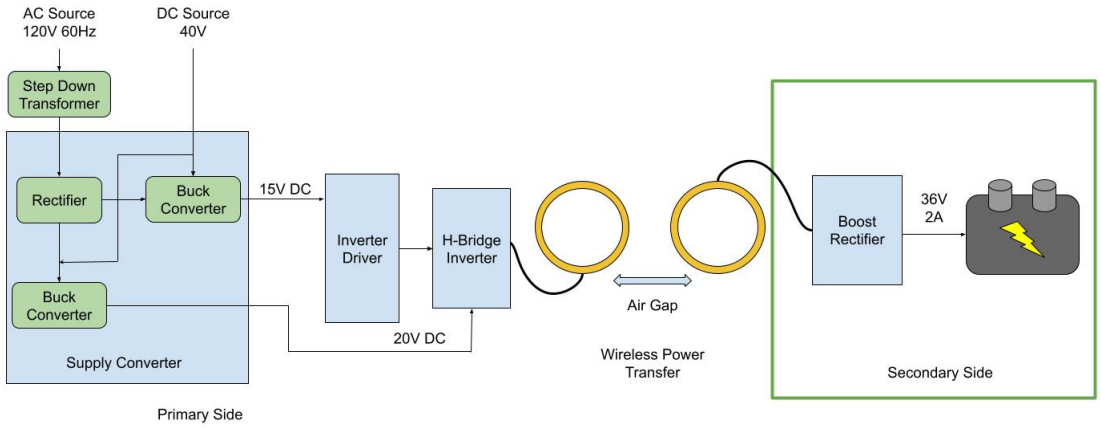

Figure 3.1: System Diagram for WPT Battery Charger

3.1.1 Choice of Transformer and Rectifier Diodes

The transformer was chosen to balance power requirements and rectified voltage level. The minimum power required is around 72 watt as the final battery charger should provide 2 amps at 36+ volts. To allow for inefficiency, a 112 watt transformer was used. This transformer produces 28Vrms at 4 amps, which in turn produces around a 45V peak. As this would produce peaks of 45

volts 60 times per second, diodes were chosen which could repeatedly withstand these currents and voltages. In addition to the repeated performance, during initial startup the diodes must withstand much higher currents as the rectifying capacitors are filled. Finally, capacitors were chosen to provide stable output voltage as our required load current is drawn. Estimations of the ripple on the voltage were made using the effective time constants of the capacitors and load, and then this was tested through simulations with a peak load.

3.1.2 Design of Inverter Driver and H-Bridge Inverter

The inverter driver has the goal of producing two switching signals, each of which is provided to a low switch and a high switch, in order to produce an output signal that alternates between a low voltage and a high voltage. The four switches are positioned in two branches, and they switch such that either the high or the low switch on a particular branch will be turned on at any one point, and the complimentary switch on the other branch will match. The critical parts of implementing this are level shifting and overlap deadtime. The deadtime refers to the fact that in one branch, it is a critical failure if both the high and low switch are activated at the same time, as this will result in a short circuit between the power supply and the ground. Achieving four signals that are synchronized (between branches) and non overlapping (within branches) is difficult and dangerous using entirely discrete components. Often, the control of switches such as these is accomplished through the use of a microprocessor, but in that case we would need an additional discrete level shifter to control the high switches, and would add additional complexity to the design.

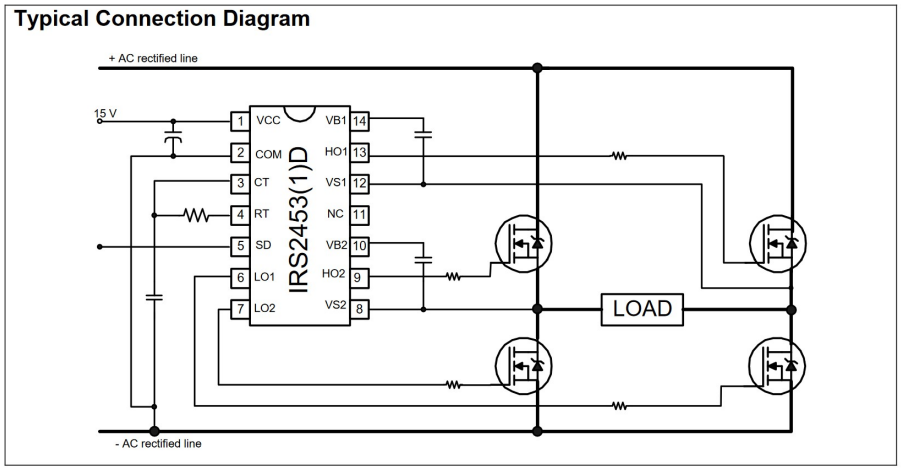

Figure 3.2: Inverter Driver Schematic [9]

Instead, an integrated self-oscillating gate driver, the IRS2453(1)D was used, implemented as shown in [9]. This chip is able to create a configurable clock signal through the selection of a timing capacitor and resistor, and it produces four non-overlapping clock signals, two of which can be level shifted relative to the required signal. This level shifting is done through an internal bootstrap diode connected to an external bootstrap capacitor, which is able to charge when the output switching node is pulled low, and then provides charge for the control of the high switch when pulled high. Internal dead-time circuitry prevents short circuits, and it can withstand the full voltage of inversion.

3.1.3 Design of Inverter Driver Level Buck Converter

For the 20V inverter switching level supply, the LM5088 [10] chip was chosen for its wide input range and safety precautions, which help protect the chip from shorts later or fluctuations in the rectifier output. This buck converter needs to produce at least 4A at 20V, and a switching frequency of 295kHz was chosen to provide low ripple while operating in the chips frequency range. The switching resistor value is defined as

$$R_{RT} = \frac{\frac{1}{295kHz} - 280ns}{152pF} \approx 20.5k\Omega \tag{3.1.1}$$

The inductor value can be selected through the output ripple voltage specification. 25%

fluctuation is allowed to provide a relatively stable range for the switches on the inverter, and so the inductor was chosen as

$$L = \frac{20V}{.25 \times 4A \times 295kHz} \times (1 - \frac{20V}{60}) \approx 45\mu H \tag{3.1.2}$$

Here, a higher input voltage is used to account for a worse case supply fluctuation, and then a $47\mu H$ inductor was chosen as a more common inductor value that maintains the specification. The buck converter includes a current sensing resistor which allows for over current protection, essentially limiting the current to a maximum value. We chose to limit the current to 50% higher than the typical current, to reduce risk of damaging other components. This is done by comparing the voltage across the current sensing resistor to a $120mV$ reference, and so a sensing resistor can be chosen as

$$R_S = \frac{0.12V}{(1 + 0.5)(4A + 0.5 \times 1A) + \frac{20V}{47\mu H \times 295kHz}} \approx 15m\Omega \tag{3.1.3}$$

An emulated ramp circuit provides current controlled behavior for the buck converter, which reduces the impact of noise in the control circuit, but this introduces the choice of a ramp capacitor and resistor. The capacitor value is set by the inductor and the built in transconductance and voltage gain of the ramp emulator. It is defined by the following formula

$$C_{RAMP} = \frac{5\mu A/V \times 47\mu H}{10V/V \times 10m\Omega 1} = 1.6nF \approx 1.5nF. \tag{3.1.4}$$

A more common 1.5nF capacitor was chosen for the final design. The resistor, which adds additional slope compensation, is described by the equation

$$R_{RAMP} = \frac{7.8V - 0.8V}{20V * 5\mu A/V - 25\mu A} \approx 93.1k\Omega \tag{3.1.5}$$

Perhaps the most essential choice was the selection of resistive feedback to produce the desired output voltage. The feedback factor is found to be about 0.06 in order to achieve a 20V output. This is done with the selection of a 1.52kΩ and a 23.7kΩ resistors.

$$\frac{R_{FB2}}{R_{FB1}} = \frac{20V}{1.205V} - 1 = 15.975 \tag{3.1.6}$$

The following figure shows the final design for the inverter driver.

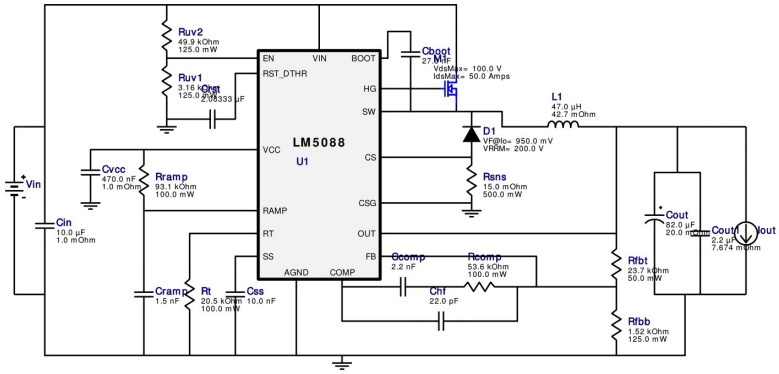

Figure 3.3: Inverter Driver Level Schematic

3.1.4 Design of Inverter Driver Supply Buck Converter

The inverter driver requires a voltage of between 12 and 16V, which is higher than the inverter voltage and must be generated separately. As such, a new buck converter is needed to produce a voltage within this operating range range. The quiescent current drawn from this source is less than 2mA, increasing up to 4mA when actively switching. As such, a more simple design with very low current requirements could be implemented. An integrated solution was chosen which produced a fixed 15V output, the LM2576HV-15.0 [11]. This chip includes the switching transistor, and so with the addition of an input capacitor, an output capacitor, a diode, and an inductor, the full buck converter is achieved. The base model can have up to 37V at the input, and as the rectifier produces 45V, the High Voltage model was chosen, which can withstand up to 60V. Using an overestimation of the load current, an inductor was chosen from the graphs provided in the TI datasheet. For the input and output capacitors, large 100uF capacitors were chosen to be have low ripple.

3.2 Design of Wireless Power Transfer System

The wireless power transfer (WPT) subsystem is designed to transfer power from the primary side to the secondary side without use of wires or other electrical connections. The subsystem is induction based transfer and is a 1 to 1 ratio from the primary to secondary side. Air gap variation was also taken into consideration in the design but constructed alignment in the final product should alleviate misalignment.

3.2.1 Selection of Coil Geometry

When AC voltage is applied to the primary side coil, the flux of the produced magnetic field couples to the secondary side and induces a voltage and current flows through the secondary system. This behavior is similar to an ideal transformer which is what was used to model the WPT system. Based on ideal transformer winding equations, the WPT was designed to have an ideal (touching) gain of x1 from the primary to secondary side. However, due to air being a poor medium, this will likely not be the case and could possibly be close to x0.5. Further improvement of this system will be made through the addition of a ferromagnetic core.

The coils used in this work were hand wound and sized to fit within the tire of a standard bicycle. A low turn count was used since the diameter was set to be large in order to have a relative inductance under 20μH. The final dimensions are given below in **Table 3.1**:

Table 3.1: Coil Dimensions

	Outer Diameter (d_{out})	**Inner Diameter** (d_{in})	**Number of Turns** (n)
Primary Coil	16.5 inches	15.25 inches	4
Secondary Coil	16.5 inches	15.25 inches	4

Using these dimensions, the inductance values of the coils were calculated using the following equation for the inductance of a circular planar coil provided by [12].

$$L_{Circ} = 31.33\mu_0 n^2 \frac{a^2}{8a + 11c} \tag{3.2.1}$$

Where L is the inductance measured in henries (H), a is the average radius of the coil, in

meters (m):

$$a = \frac{d_{in} + d_{out}}{4} \tag{3.2.2}$$

c is the width of coil, in meters (m):

$$c = \frac{d_{out} - d_{in}}{2} \tag{3.2.3}$$

μ_0 is the vacuum permeability in henries per meter (H/m),

$$\mu_0 = 4\pi \times 10^7 \tag{3.2.4}$$

and n is the number of turns. The calculated values of the hand wound coils are found in Table 3.2.

Using the method described in [13], the indctance of the wound coils was measured. The resistance of each coil was measured with a multimeter. The resulting inductances and resistances are given below in **Table 3.2**:

Table 3.2: Inductance and Resistance of Coils

	Calculated Inductance	**Measured Inductance**	**Measured Resistance**
Primary Coil	15μH	16.28μH	3.35Ω
Secondary Coil	15μH	16.95μH	3.4Ω

The measured values are within a thirteen percent margin of the calculated value The measured values were accepted as the final values and used in later calculations.

3.2.2 Coil Compensation

Maximum power transfer in an LC circuit occurs when the capacitive and inductive reactances are equal which is called resonance [14]. While operating at resonance the LC bank can store energy in the capacitor which can induce a voltage on the inductor and thus maximizes the amount of power that can be transferred in the system. In order for the inductors in this work to operate at resonance at the inverter driving frequency a compensation capacitor is added to the WPT system. There are four configurations of compensation capacitors and the inductors which are described in [15]. This work attempted to use Parallel-Parallel compensation to achieve the desired resonance operation. The value of the compensation capacitor needed was calculated using the

measured inductance values of the coils as well as the inverter driving frequency of 72kHz. Below is the equation used to calculate both the primary and secondary side compensation capacitors.

$$\omega_0 = \frac{1}{\sqrt{LC}} \tag{3.2.5}$$

3.3 Design of Secondary Side Electronics

Due to the possibility of coil misalignment as well as the losses in the air gap, the secondary side electronics were designed to have a wide input range that would also provide a stable output for charging of a battery.

3.3.1 Choice of Rectifier Diodes

The output of the WPT secondary coil is expected to be a switching waveform with an amplitude ranging from 15V to 30V depending on the coils performance. The induced current that would flow into the secondary side electronics could range from 2A to 5A and thus the diodes used in the secondary side rectifier were chosen to meet these ratings. The Panjit MBR20200CT-T0-00001 was chosen as its ratings of a 200V Repetitive Reverse Voltage and a maximum forward current of 10A give plenty of headroom for the variable output of the secondary coil.

3.3.2 Design of Boost Converter

The main design considerations for the output boost converter are its input voltage range, output voltage and current, as well as converter efficiency. The input voltage for the secondary side boost converter could range from 15V to 30V based on the losses on the diode bridge. When charging a typical 36V battery, usually the charger output voltage is held at a higher value than 36V, depending on the rating of the battery. For this design, a 36V battery with a charging voltage of 40V will be used for testing so the output voltage of the boost converter was set at 40V. Below is a table of the design variables used to create the boost converter.

To achieve the desired high efficiency operation, an IC is used as the control unit for the boost converter topology. The LM3478MMNOPB by TI was a reliable and inexpensive option for this converter and the boost converter components were designed following this chip's operating

Table 3.3: Boost Converter Design Variables

Variable	**Value**
Minimum Input Voltage	15V
Maximum Input Voltage	30V
Output Voltage	40V
Output Current	2A
Converter Efficiency	90%

parameters as listed in [16]. The design began by calculating the expected duty cycle (D) of the boost converter based on the input and output voltages. The duty cycle of a boost converter is defined as

$$D = 1 - \frac{V_{In}}{V_{Out}}. \tag{3.3.1}$$

Using equation 3.3.1 the maximum and minimum duty cycle were calculated. The next step is calculating necessary inductor value for continuous conduction mode (CCM) operation. A switching frequency (f_s) of 0.5MHz was chosen to keep the inductor small. Using this frequency, the minimum duty cycle, the maximum input voltage and Iout which is defined in Table 3.3, the minimum inductor value is calculated as follows

$$L > \frac{D(1-D)V_{In}}{2I_{Out}f_s} = 2.62\mu H. \tag{3.3.2}$$

The current ripple on the inductor ($\Delta I_{L(max)}$) also has an impact on the size of the inductor. Typically a ripple of 20% of the Average I_L is chosen. The peak inductor current also determines the ratings of the inductor. The inductor value from this current ripple guideline as well as the peak inductor current are calculated as follows.

$$Average\ I_{L(max)} = \frac{I_{Out}}{1 - D_{max}} = 5.6A \tag{3.3.3}$$

$$\Delta I_{L(max)} = 0.2 \times Average\ I_{L(max)} = 1.12A \tag{3.3.4}$$

$$L = \frac{D_{max} \times V_{Inmin}}{2 \times f_s \times \Delta I_{L(max)}} = 8.17\mu H \tag{3.3.5}$$

$$I_{LPEAK} = Average\ I_{L(max)} + \Delta I_{L(max)} = 6.72A \tag{3.3.6}$$

The next components of interest are the feedback resistors used to set the output voltage. These resistors are selected such that the FB pin on the LM3478 is at 1.26V through the voltage division between the resistors. Selecting R_{F1} as 30.9kΩ, the following equation is used to find R_{F2}

$$R_{F2} = \frac{1.26 \times R_{F1}}{V_{Out} - 1.26} \approx 1k\Omega \tag{3.3.7}$$

Another key component for the boost converter as the interface for the battery charger is the R_{SEN} resistor that sets the maximum output current the converter can supply. When the voltage across R_{SEN} is equal to the current sense threshold voltage V_{SENSE}, the switch will be turned off until the next cycle. Using the V_{SENSE} and V_{SL} ratio given in the electrical characteristics of the LM3478, the R_{SEN} resistance is calculated as follows

$$R_{SEN} = \frac{V_{SENSE} - (D \times V_{SENSE} \times V_{SL}\ ratio)}{ISW_{LIMIT}} \tag{3.3.8}$$

Where

$$ISW_{LIMIT} = \frac{I_{Out}}{1 - D} + \frac{D \times V_{In}}{2 \times f_s \times L}. \tag{3.3.9}$$

The MOSFET was selected based on voltage and current characteristics as well as a low RDS for decreased switching loss. The input capacitor is used for filtering of the input current fed through the inductor. Its value was chosen based on suggested designs along with a bypass capacitor to further reduce IC noise. The power diode used in the boost converter needed to be rated for the peak diode current that is calculated below.

$$I_{D(PEAK)} = \frac{I_{Out}}{1 - Dmax} + \Delta I_L = 6.72A \tag{3.3.10}$$

Thus the same diode used in the secondary rectifier was used for convenience. The final component value and rating that was considered was the output capacitance. The output capacitor

is responsible for controlling the output voltage ripple and thus should be chosen to handle output current ripple maximums while reducing voltage ripple. The RMS current in the output capacitor can be calculated as follows

$$I_{COUT(RMS)} = \sqrt{(1 - Dmax)[I_{Out}^2 \frac{Dmax}{(1 - Dmax)^2} + \frac{\Delta i_L^2}{3}]} \tag{3.3.11}$$

Where

$$\Delta i_L = \frac{Dmax \times V_{In}}{2 \times L \times f_s} \tag{3.3.12}$$

This gives an $I_{COUT(RMS)}$ of approximately 4A rms and thus output capacitors rated for 5A rms were chosen. A capacitor with a low ESR is chosen for high efficiency and low output ripple voltage. The following schematic has the final component values used in the construction of the output boost converter.

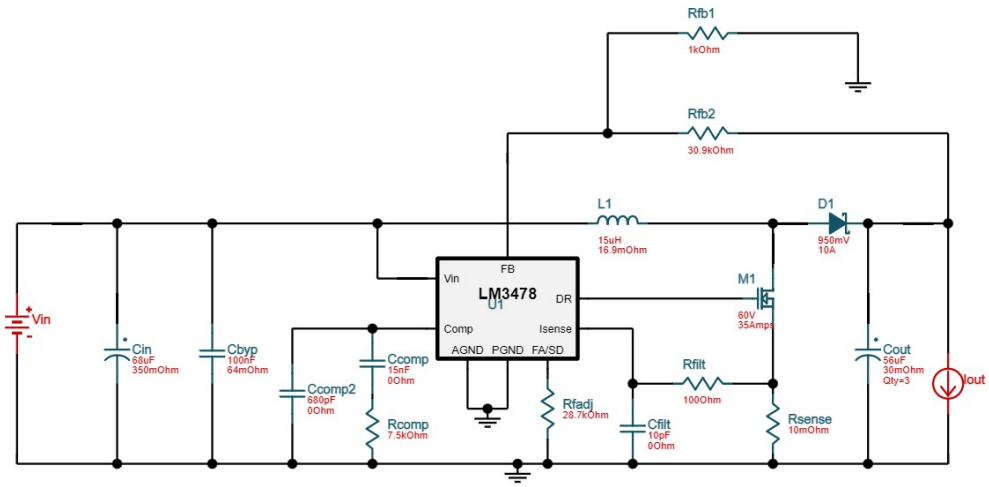

Figure 3.4: Output Boost Converter Schematic

4. RESULTS

In this chapter we discuss the results from the simulations of the designed electronics components as well as the data gathered from a constructed prototype. Since this is foundation of this project type, these results are considered fundamental and will be built upon by later researchers.

4.1 Simulation Results

4.1.1 Primary Side Electronics

The primary side consists of four main components: the rectifier, the inverter driver supply buck converter, the inverter control buck converter, and the inverter itself. The inverter did not have any simulation model available for tests, but simple switching signals were used to approximate its output, resulting in inversion of a DC voltage. The LM2576HV-15 was simulated using a SPICE model provided by TI, which showed operation that created 15V at currents exceeding the expected load. The LM5088 chip was simulated using TI's TINATI software, which allowed us to test startup and steady state cases for performance.

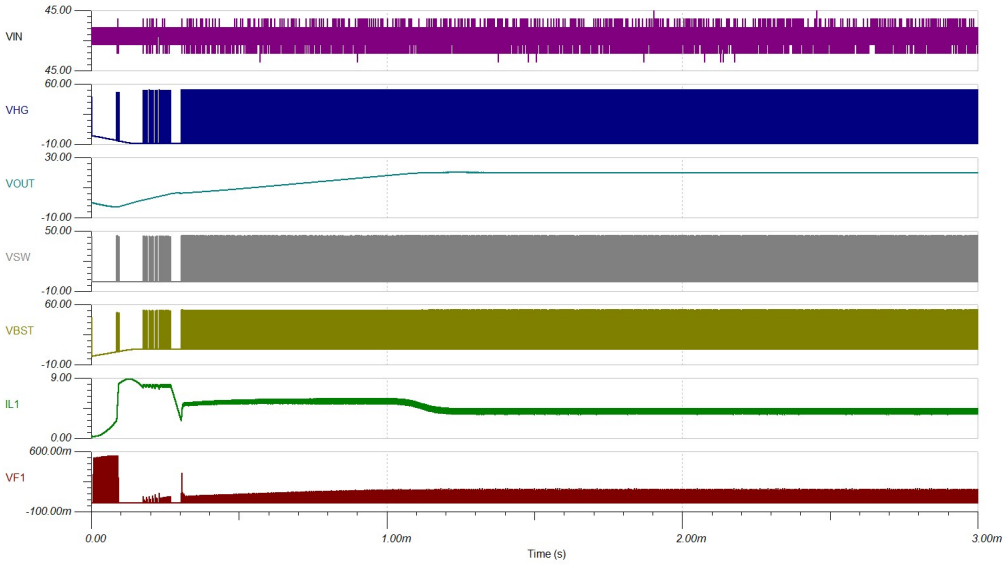

Figure 4.1: LM5088 Buck Converter Simulation

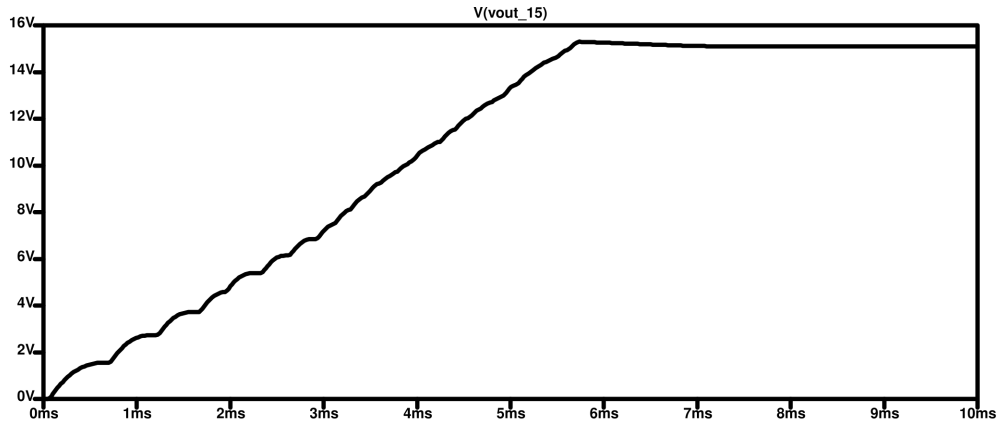

Figure 4.2: LM2576HV-15 Buck Converter Simulation

The simulation for the LM5088 buck converter show it has low ripple at high current draw, meaning it should be able to provide as much current as is needed to drive the inductor. The LM2576HV-15 displays a very steady output voltage at medium current draw, which is much higher than the actual use case. This is important, as a voltage over the inverter control chip's upper threshold can trigger the breakdown voltage of the internal diode, which would result in a short circuit of the control's power, and stop the inverter operation.

4.1.2 Secondary Side Electronics

The main component of the secondary side electronics is the boost converter. Since the rectifier is a relatively simple circuit, its simulation validation was excluded from this work to instead focus on the boost converter. As stated in the design section, the secondary side electronics was designed to help stabilize the output of the charger. Possible misalignment of the WPT coils should be compensated by this boost converter who's efficiency and input range were the most significant design factors. It is for those reasons that the TI LM3478 High-Efficiency Low-Side N-Channel Controller for Switching Regulator IC was chosen as the driver of the boost converter. TI's WEBENCH Power Designer software was used to simulate the output boost converter. The steady state voltage at a full load of 2A is displayed in the figure below. The simulated voltage ripple amplitude is around 0.1V around the average value of 40.1V which would be less than 1%. This result should be sufficient for charging a battery at approximately 80W.

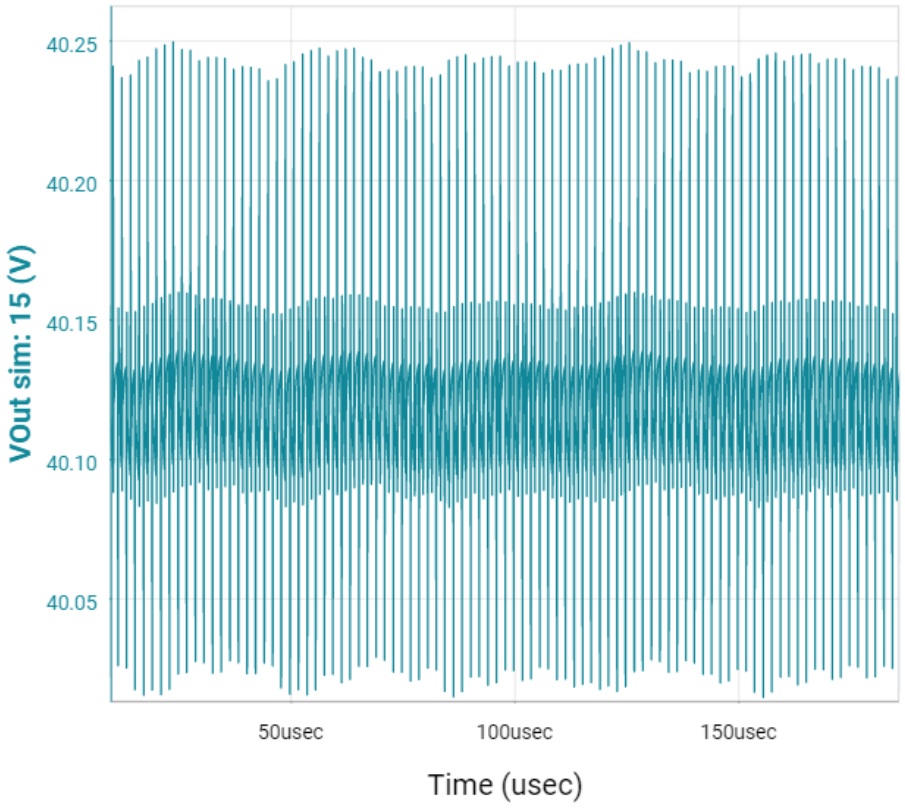

Figure 4.3: Boost Converter Simulated Steady State Output Voltage

Another important characteristic to consider is the startup behavior of the boost converter. Since the power transfer through the coils is limited, we have to consider the required startup currents and voltages for boost converter operation. Below are both the output and input simulated voltage and current waveforms. Although originally considered negligible, the large input current spikes during startup seem to have caused issues in the prototype functionality. The peak after 2ms of about 10A caused issues at high load start up due to the coils not driving enough current. This issue and possible solutions are discussed in the following sections. The startup behavior of the input and output voltage as well as the output current were as expected, with the longer build up of the output voltage stemming from the lowest input setting of 15V leading to a longer period of switching in order to reach 40V.

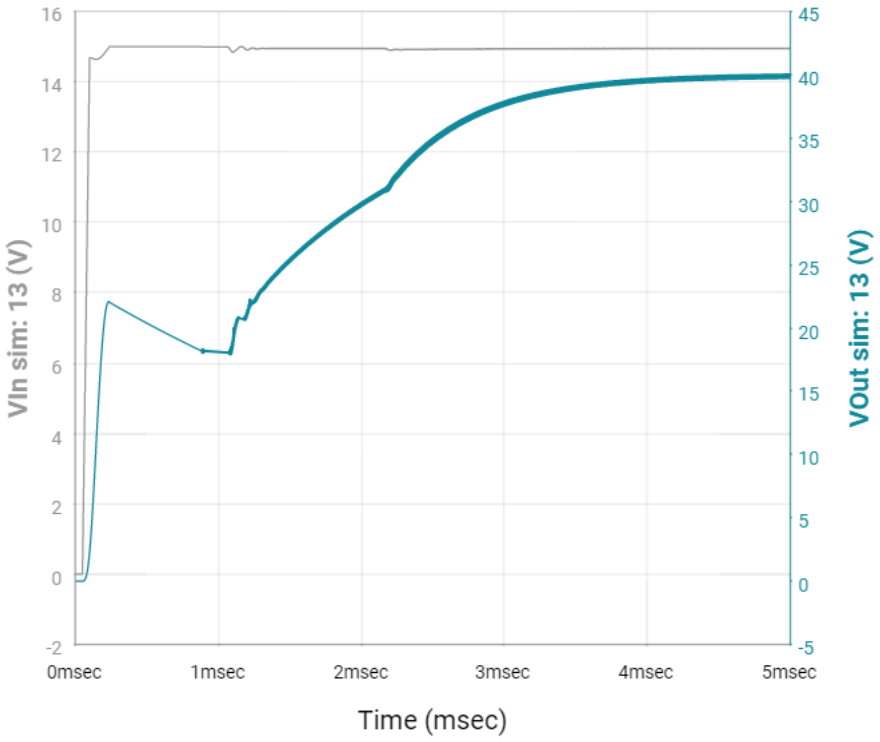

Figure 4.4: Boost Converter Simulated Start Up Voltages

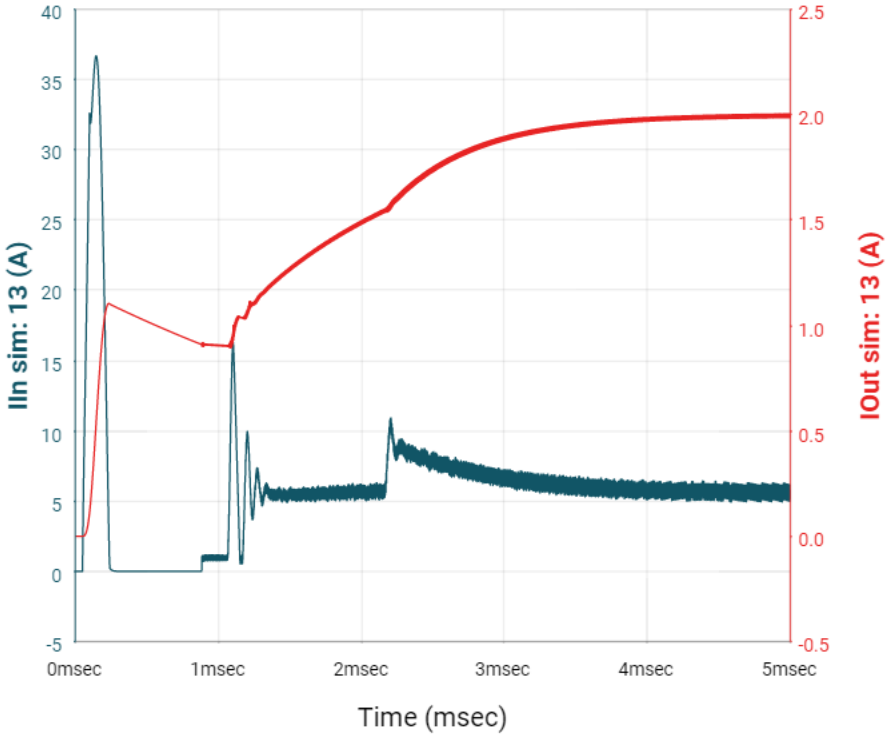

Figure 4.5: Boost Converter Simulated Start Up Currents

The next simulations performed on this boost converter design were an input and load transient simulations. The input transient shows how the boost converter would react to a sudden misalignment of the coils as well as the realignment. As seen in the figure below, the boost converter is able to maintain a voltage above 39.6V when the input suddenly changes after an initial boosted period. The ripple of the output voltage does increase at lower input voltages but is still below 1% of the average output.

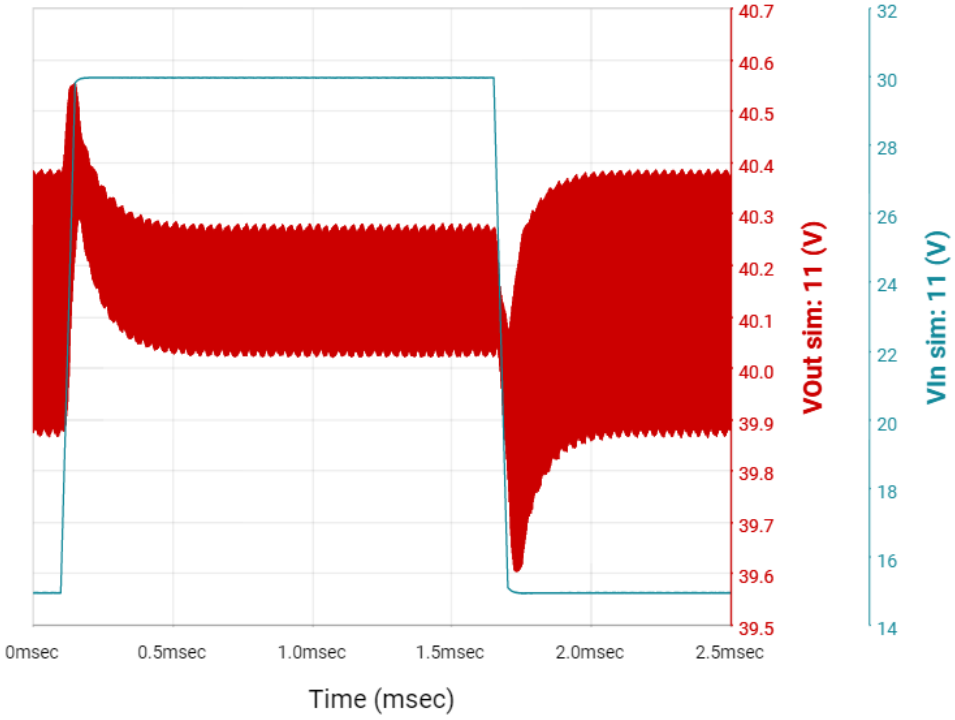

Figure 4.6: Boost Converter Simulated Input Transient

The load transient simulation was conducted as a reference point for when the secondary side is pulled away or initially coupled to the primary. When there is a light load (low output current) the boost converter is able to reach a higher output voltage that is closer to 41V rather than the originally desired 40V. But with a sudden change in output current demand, the output voltage drops to 38.2V and the controller has to once again boost up to the 40V output. This drop should not be a problem when initially attaching a battery as the voltage is above the nominal 36V battery voltage and thus should allow charging to occur regardless.

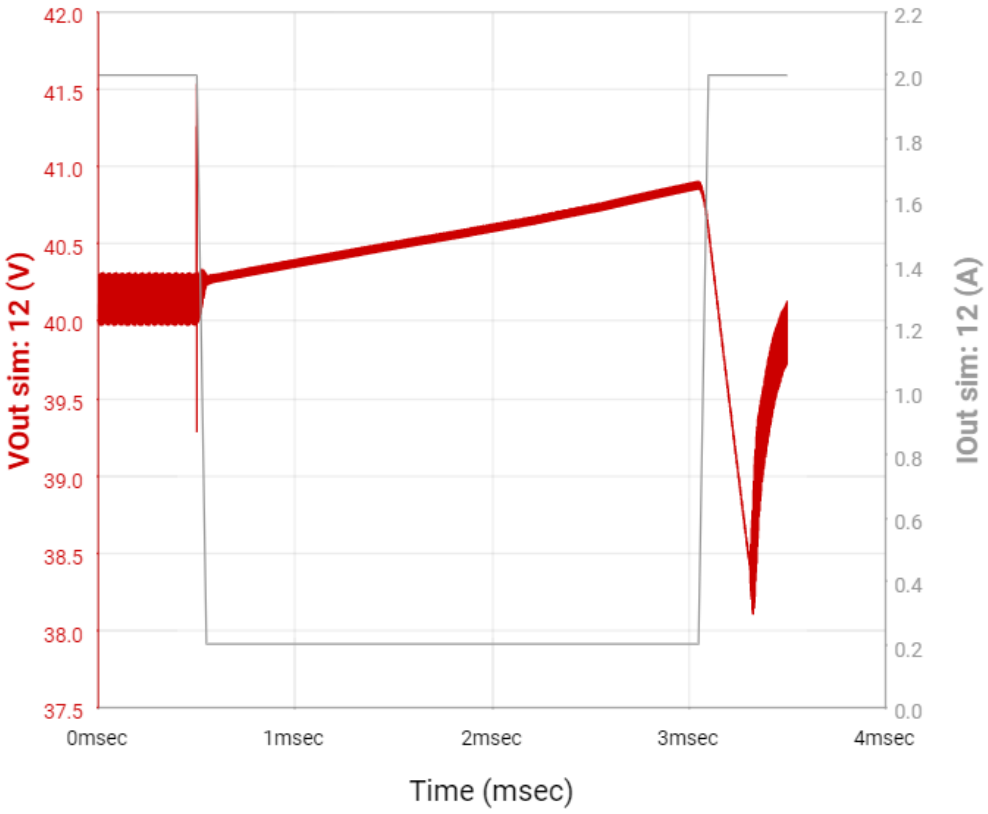

Figure 4.7: Boost Converter Simulated Load Transient

Finally, the efficiency of the converter was plotted at different input voltages as a function of the output current. The plot below shows that efficiency is expected to be above 95% at all voltage and current level and peaks at approximately 96.6% for an input voltage of 30V.

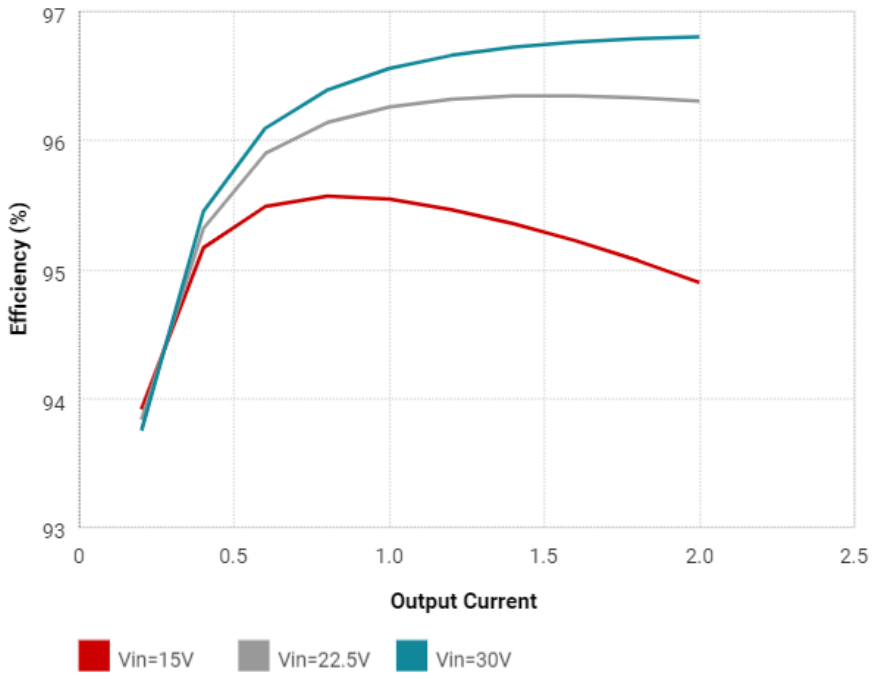

Figure 4.8: Output Boost Converter Simulated Efficiency

With these simulation results, especially the high efficiency ratings, the output boost converter design was deemed suitable for the prototype application and thus was implemented into the system as discussed in the next section.

4.2 Prototype Test Results

4.2.1 Primary Side Electronics Prototype Verification

To test the primary prototype, two categories of test were performed. The first category was basic functional tests, to check if the appropriate voltage and inversion was being created. These tests were performed with both DC and AC inputs, which showed the same results as seen below. The resulting inverter output waveform has a switching frequency of approximately 72kHz which is the frequency at which the coils will operate.

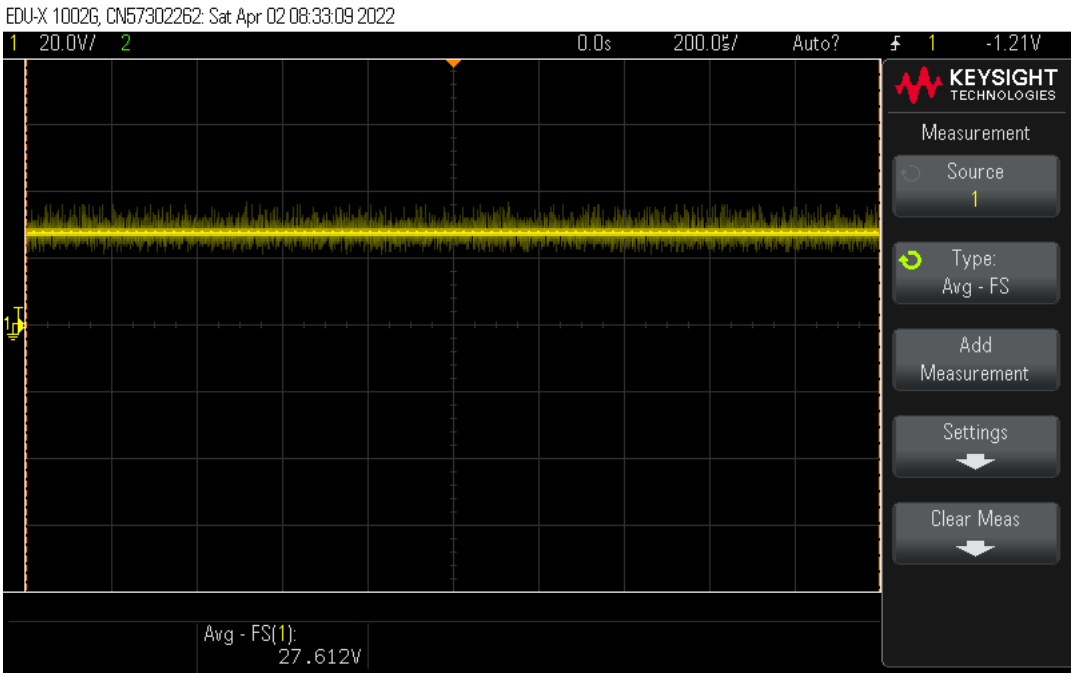

Figure 4.9: Buck Converter Output

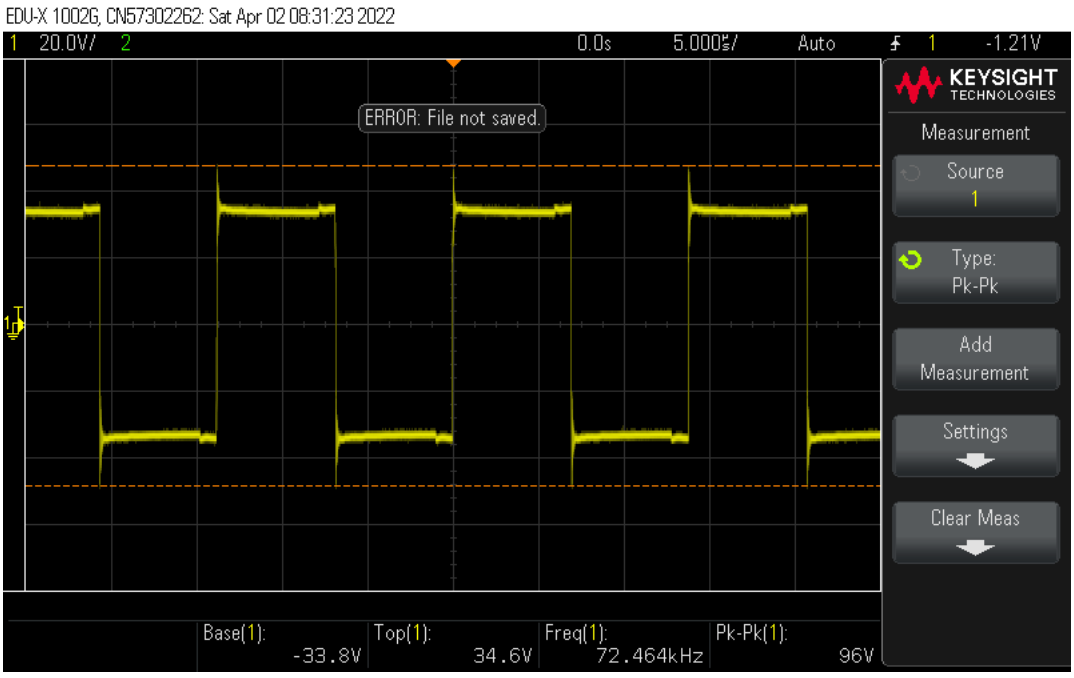

Figure 4.10: Inverter Output

Following the successful completion of these tests, load tests were performed to find the maximum load current and power that could be supplied by the primary electronics. This test

was performed by attaching a variable resistor, or potentiometer to the output of the inverter. The resistance of the potentiometer was measured using a digital multimeter, then a DC voltage was supplied to the primary electronics, and the RMS voltage across the resistor was measured using an oscilloscope. Then the resistance was decreased, and the process repeated. The buck converter maintained close to full output voltage for the maximum load we could achieve using this potentiometer.

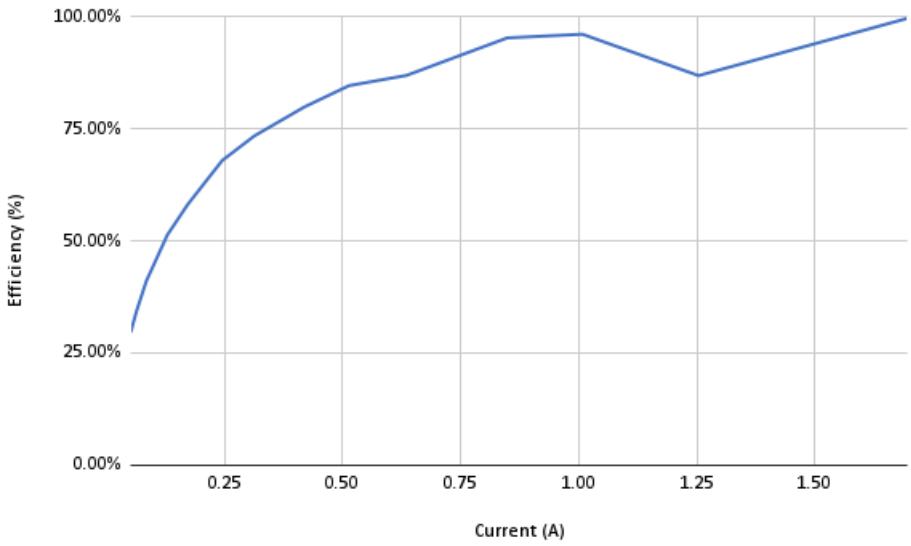

Figure 4.11: Inverter Output Efficiency across load current

4.2.2 Inductive Coils

The inductors were tested in a similar manner, first performing a simple operational test with low load current, and then increasing load to find the maximum deliverable power. The RMS output voltage was measured across load currents, and the current was found using the measured resistance.

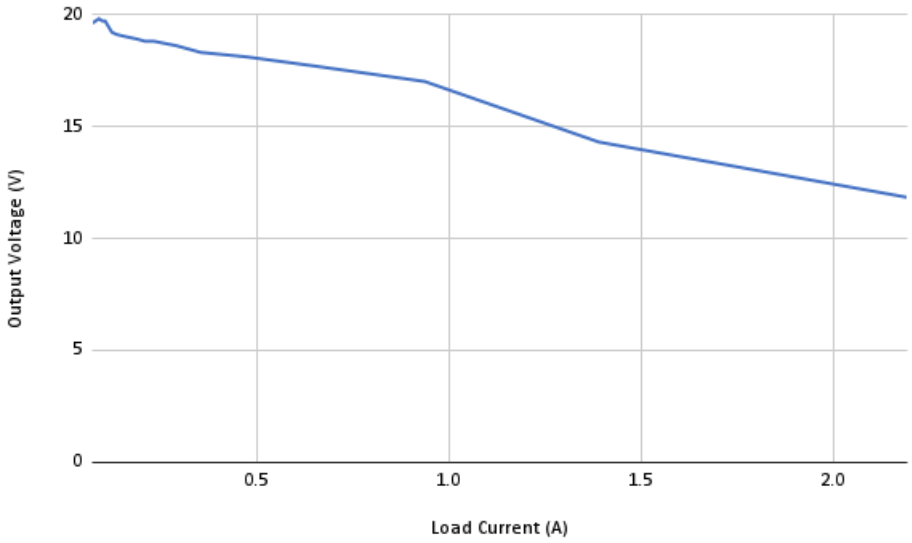

Figure 4.12: Basic Coil Output

The decline in output voltage at higher currents provides an upper bound on the power transferred through the inductive coupling. We noticed minimal decline in the output voltage up until 1A load, at which point there was a sharp decrease in output voltage. At the maximum tested load, the output voltage has decreased nearly 50%, which provides a limit at the input to the secondary stage electronics.

4.2.3 Secondary Side Electronics Prototype Verification

The secondary side electronics were tested individually by supplying a DC voltage to the input of the boost converter. Multiple DC inputs were tested to ensure the wide range input voltage design worked at light load. An example of the light load output voltage of the converter driven with a 25V input is shown below.

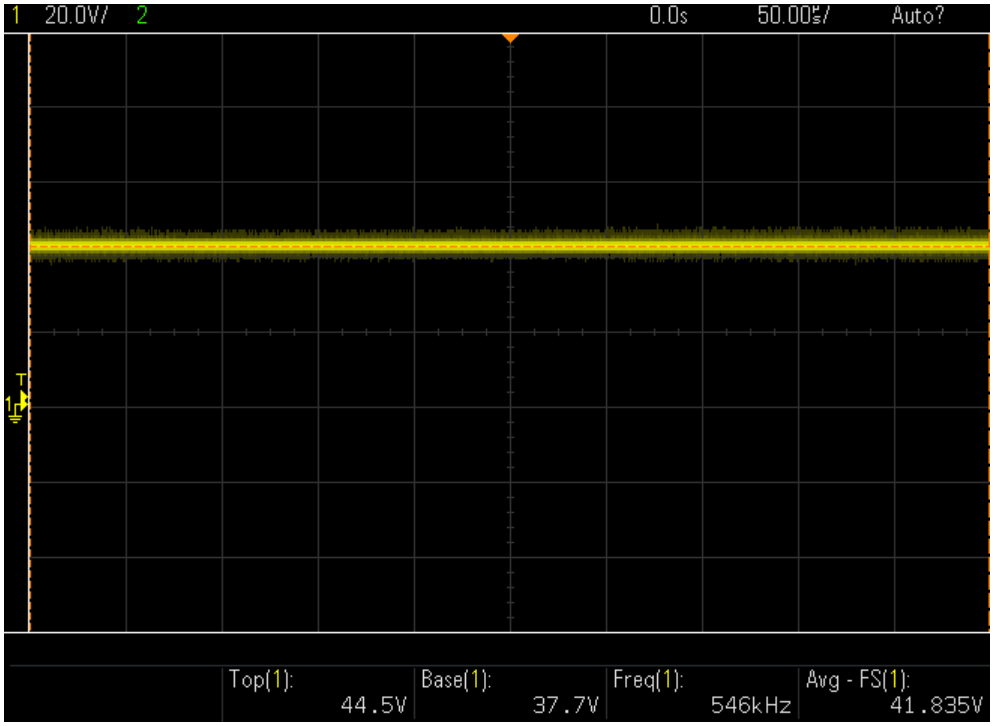

Figure 4.13: Boost Converter Output Voltage at Light Load

Load transient tests were also performed on the boost converter and showed issues with high loads over 1A. The maximum output current achieved before system shut down was 1.21A at 40V with an input of 25.1V and 3.2A. This was an efficiency of only 47.7% which is much lower than anticipated in the design. The likely causes for this malfunctioning are overheating of the transistor and IC controller or an issue with an inaccurate sense resistor causing the chip's current control to improperly set the chip function. As mentioned previously, this project will be ongoing but results from light load measurements seem promising as a solution to stabilizing the output voltage levels, which is a top priority for a battery charger. The majority of data collection was carried out as part of full system validation which is covered in the next section.

4.2.4 Full System Prototype Verification

The full system verification was conducted in two main steps. The first step was using the initial design of the primary side inverter, inductive coils, and the secondary rectifier and boost converter. After this initial testing, compensation capacitors were used to reach resonant power

transfer in hopes of further improvement. Below is a diagram of the test set up used during experimentation.

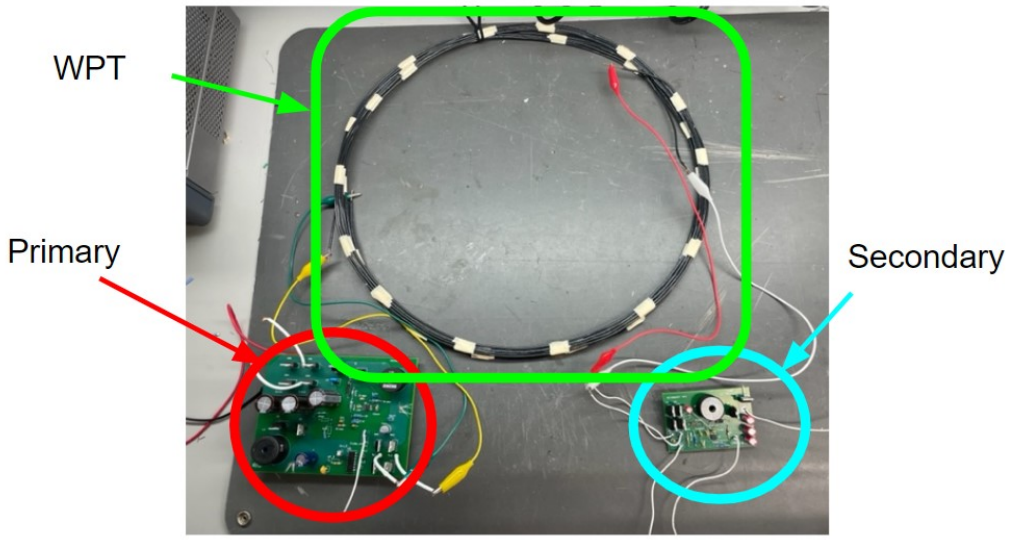

Figure 4.14: Prototype Set Up

4.2.4.1 Initial Test Results

This test acted as the proof of concept for the wireless charger. The primary side inverter was attached directly to the primary side coil which had the secondary coil stacked on top of it, thus giving minimum distance. The secondary coil was attached to the secondary side electronics which was loaded with a 100W 500 Ω potentiometer. The light load functionality of the system was tested first and waveforms of the primary and secondary coil voltages as well as the output voltage were captured and are shown below. As previously stated, there is a loss in voltage level from the primary to the secondary coil due to the losses in the air core. But even with this loss, the system is still able to boost to a 42V output under light load conditions. The output voltage ripple is larger than in simulation but still under 10% of the average output value. These results were similar for both the AC and DC input source, so further testing was done using the DC input for better input power measurements.

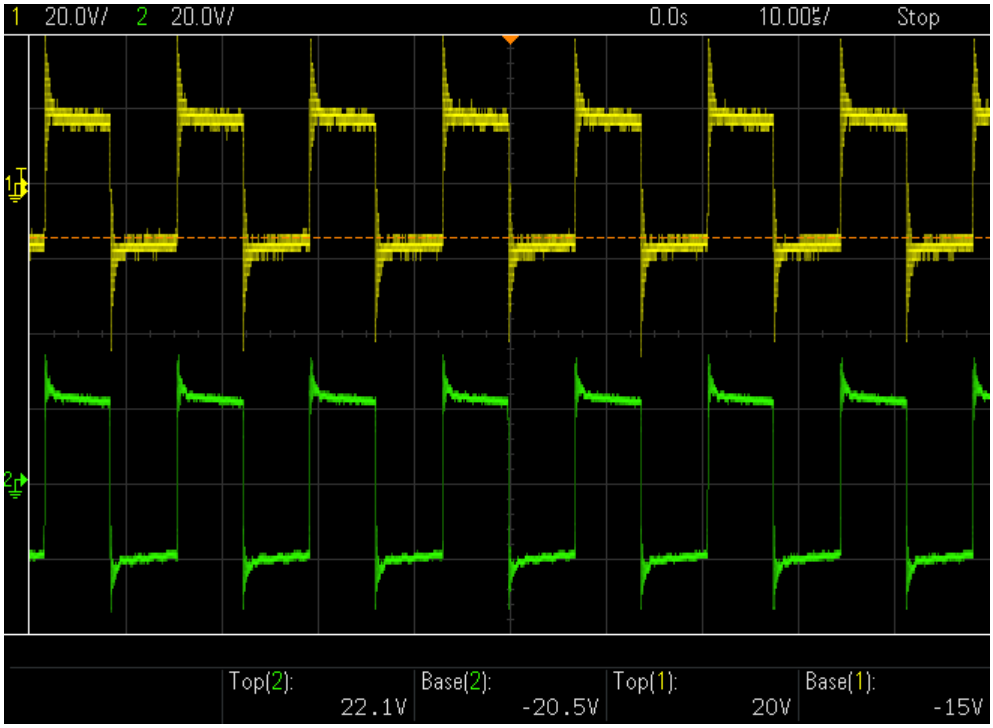

Figure 4.15: Primary Coil Voltage (CH2) Secondary Coil Voltage (CH1)

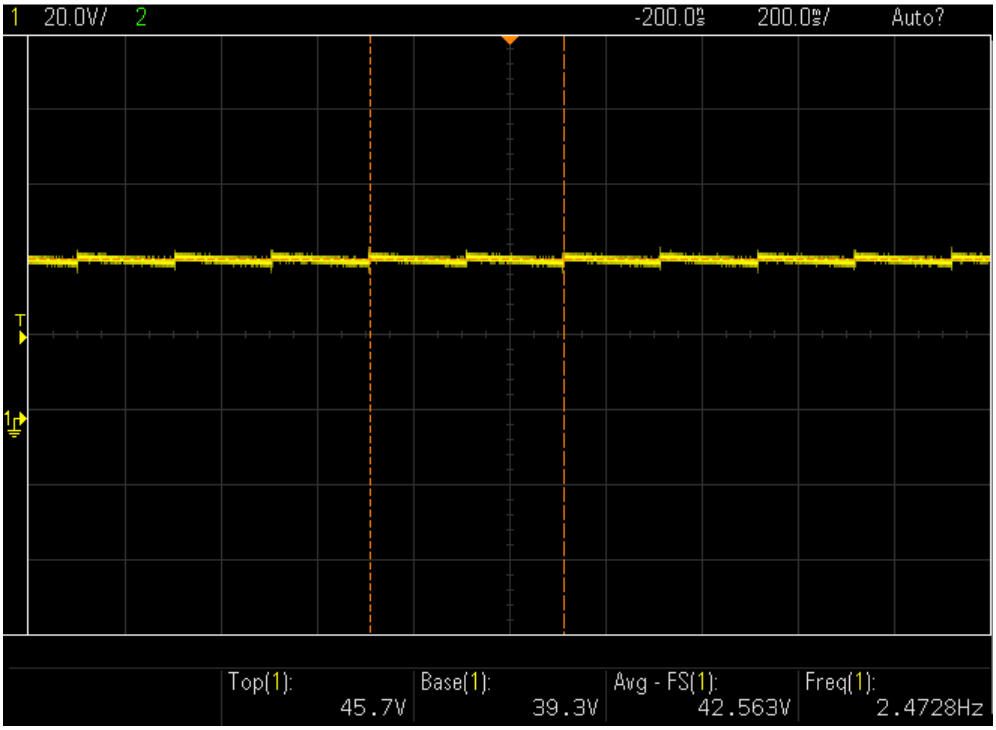

Figure 4.16: Output Voltage of Full System at Light Load

Misalignment tests were also performed on the light load system. This test found the maximum separation distance for the primary and secondary coils as well as the maximum misalignment while touching for the boost converter to maintain a 40V output. The table below includes these maximum values.

Table 4.1: Misalignment Measurements

	Measurement
Maximum Coil Separation Distance	2.54 cm
Maximum Misalignment	5 cm

Using a high power DC supply to power the primary electronics, load transient data was gathered through oscilloscope measurements of the output voltage on a multimeter measured output resistance. The first chart displays the achieved output power as a function of the load current. Since the slope of the line is 40V, one can see that the output voltage was held constant throughout the load changes. After approximately 0.4A output current, the secondary side shut down due to current limitations from the WPT.

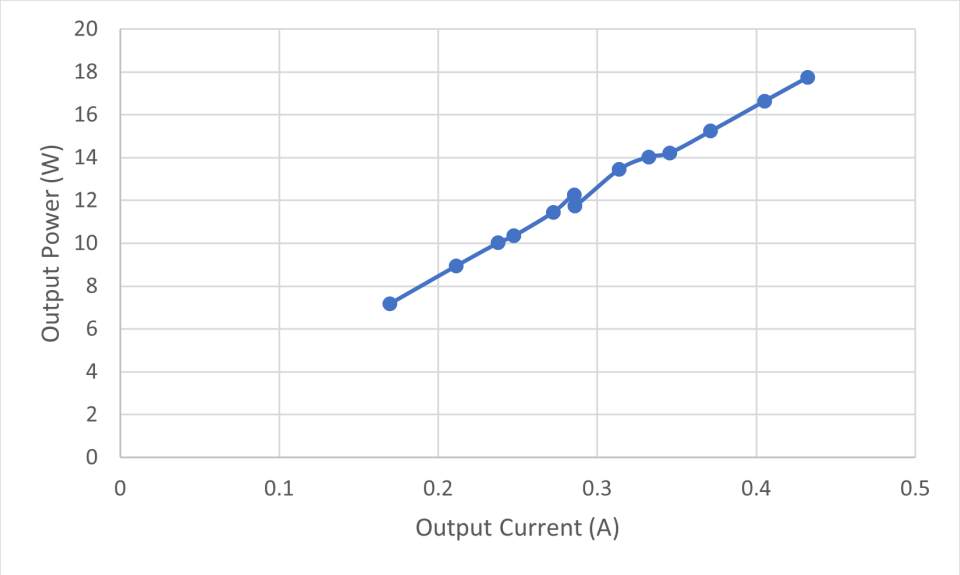

Figure 4.17: Measured Output Power vs Output Current

The efficiency of the full system was also recorded and is charted as a function of load current in the following figure. The maximum efficiency reached for a steady 40V output was

approximately 53.2% at a load current of 345mA. After this point the efficiency of the charger decreased until limiting the output after a load current of 430mA and efficiency of 50.6%.

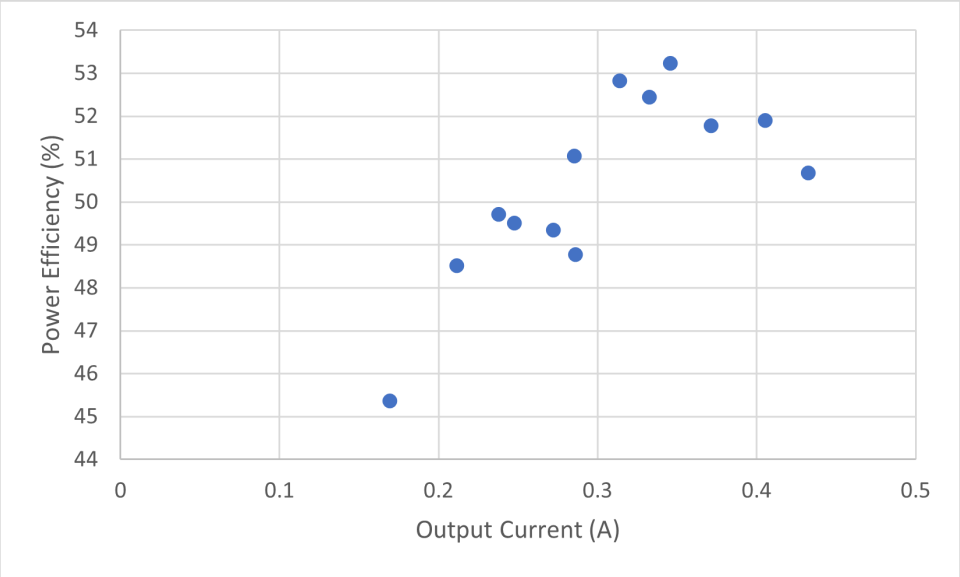

Figure 4.18: Measured Power Efficiency vs Output Current

The system faced an issue with reaching high load currents. The charger was originally designed with the goal of 2A output current but could not get past 0.4A before current limiting. This lead us to believe the coils were incapable of delivering enough power to the secondary system through the induced magnetic field. To increase maximum power transfer, the coils were then tuned to approximately resonance using parallel capacitors. The results are covered in the next section.

4.2.4.2 Compensated Resonant WPT Test Results

The primary and secondary coils were attached to their respective resonant capacitor value for a 72kHz input frequency in a parallel configuration. This addition resulted in a significant increase in secondary side voltage. As seen in the figure below, the voltage on the primary and thus transmitted to the secondary side significantly increased and also adapted a sinusoidal waveform. The max value of the compensated secondary side voltage is nearly 70V under light load which is indicative of the improvements in power transfer when operating at resonance.

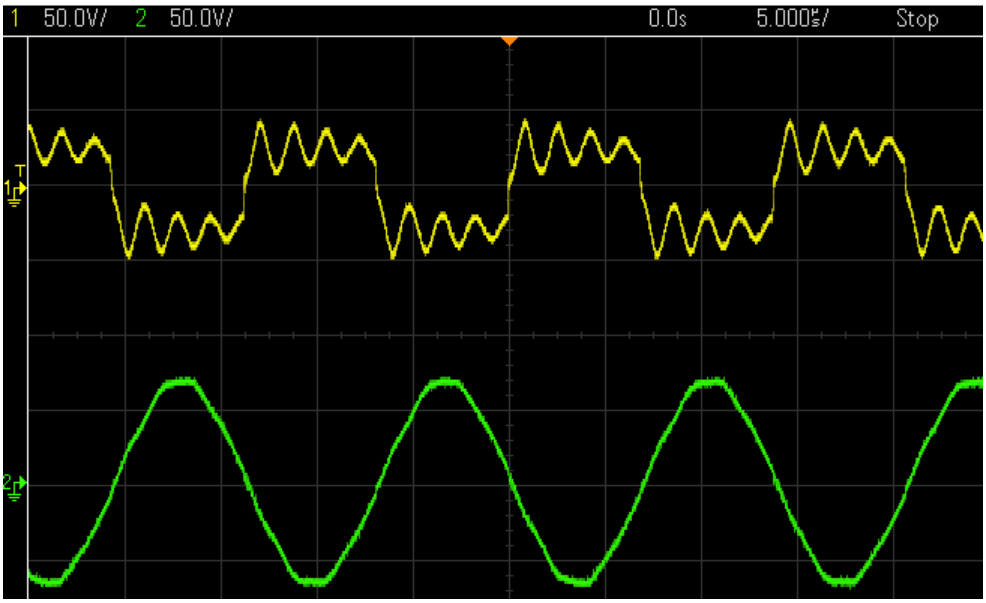

Figure 4.19: Measured Output Power vs Output Current

Using the same set up as before but with the addition of parallel capacitors, another set of varying load measurements were taken. As seen in the graphs below, the efficiency and output power of the system did increase, albeit not to the originally desired levels.

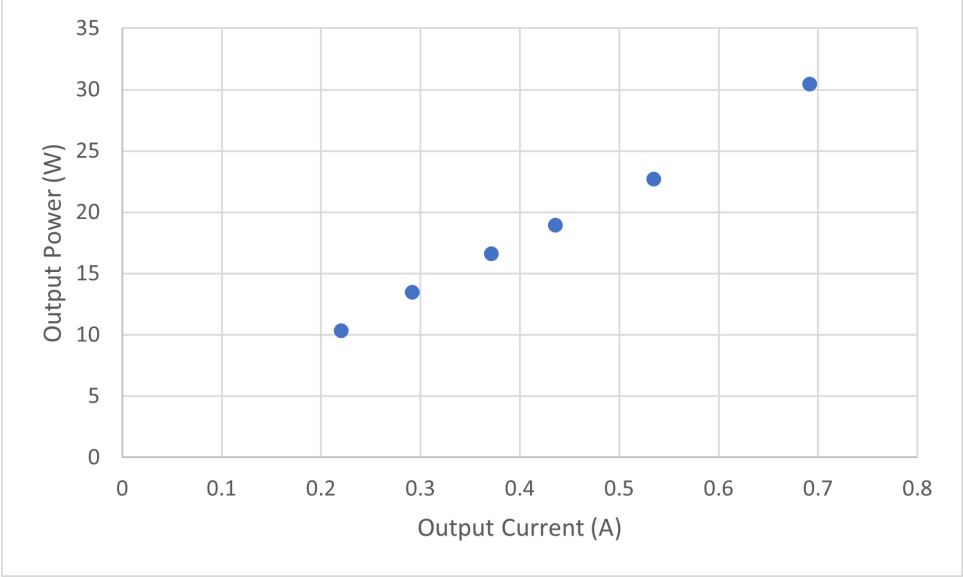

Figure 4.20: Measured Compensated Output Power vs Output Current

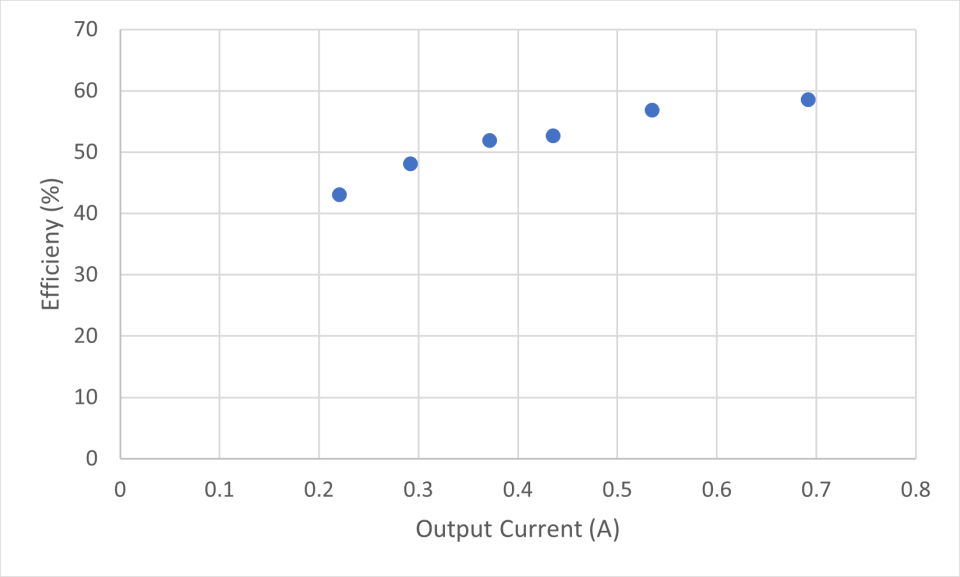

Figure 4.21: Measured Compensated Efficiency vs Output Current

With the addition of parallel capacitors, we see a maximum output power of 30W at 690mA compared to the 17W at 432mA for the initial configuration. This is 76% increase in output power which gives hope that further improvements could still be made. The efficiency of the compensated system maxed out at 58% which is a bit closer to the desired 90%. The output current still remains under half of the desired 2A output but would still be able to slowly charge a battery. After the maximum output current was reached, the secondary side boost converter began to current limit once again. Other attempts at improvement were made, such as attempting to use larger inductance coils for stronger magnetic fields, however these efforts did not fully reach their fruition and were eliminated from this work. Below is a comparison table of the values collected in this work.

Table 4.2: Comparison of Configurations

Configuration	**Value**	**Measurement**
Non-Compensated	Max Efficiency	53.2%
	Max Output Current	432 mA
Compensated for 72kHz Resonance	Max Efficiency	58%
	Max Output Current	690 mA

The final design results for the compensated configuration and operating values are listed in the following table.

Table 4.3: Design Results and Operating Values

Name	**Value**
DC Input Voltage	40V
AC Input Voltage	30Vrms
Max Input Power	52W
Operating Frequency	72kHz
DC Output Voltage	40V
Max Output Current	690 mA
Max Output Power	30.4W
Max Power Efficiency	58%

The compensated configuration was taken as the final design for this work but will be further improved by later works.

5. CONCLUSION

This work serves as the groundwork for future exploration of wireless power transfer. Essential first steps have been taken, such as successfully implementing the dual source power input and successfully achieving wireless power transfer. Additionally, the boost converter provided a more stable output across a wide range of loads, but further investigation into the integration between the inductive coils and the boost converter could yield more detailed information about how to improve the power delivered. Comparisons between resonant and non resonant WPT are also made and establish the impact of compensation. More research into the inductors and inverter control is necessary to improve the power supplied through the air gap.

REFERENCES

[1] A. Triviño, J. M. González-González, and J. A. Aguado, "Wireless power transfer technologies applied to electric vehicles: A review," *Energies*, vol. 14, no. 6, 2021.

[2] S. A. Q. Mohammed and J.-W. Jung, "A comprehensive state-of-the-art review of wired/wireless charging technologies for battery electric vehicles: Classification/common topologies/future research issues," *IEEE Access*, vol. 9, pp. 19572–19585, 2021.

[3] W. Lin and R. W. Ziolkowski, "Electrically small huygens dipole array for 5g wireless power transfer enabled iot applications," in *2020 International Symposium on Antennas and Propagation (ISAP)*, pp. 587–588, 2021.

[4] G. Guidi, A. M. Lekkas, J. E. Stranden, and J. A. Suul, "Dynamic wireless charging of autonomous vehicles: Small-scale demonstration of inductive power transfer as an enabling technology for self-sufficient energy supply," *IEEE Electrification Magazine*, vol. 8, no. 1, pp. 37–48, 2020.

[5] D. K. Babaahmadi, M. Hamzeh, and S. Farhangi, "Performance improvement of control system for wireless charging of electric vehicle," in *2021 12th Power Electronics, Drive Systems, and Technologies Conference (PEDSTC)*, pp. 1–5, 2021.

[6] Z. Yan, Y. Zhang, T. Kan, F. Lu, K. Zhang, B. Song, and C. C. Mi, "Frequency optimization of a loosely coupled underwater wireless power transfer system considering eddy current loss," *IEEE Transactions on Industrial Electronics*, vol. 66, no. 5, pp. 3468–3476, 2019.

[7] X. Lu, P. Wang, D. Niyato, D. I. Kim, and Z. Han, "Wireless charging technologies: Fundamentals, standards, and network applications," *IEEE Communications Surveys Tutorials*, vol. 18, no. 2, pp. 1413–1452, 2016.

[8] F. T. Ulaby, M. M. Maharbiz, and C. Furse, "Circuit analysis and design," 2018.

[9] Infineon, *Integrated 600V Full Bridge Gate Driver IC*, 2016. Rev. D.

[10] Texas Instruments, *Wide Input Range Non-Synchronous Buck Controller*, 2014. Rev. X.

[11] Texas Instruments, *Series SIMPLE SWITCHER® 3-A Step-Down Voltage Regulator*, 2021. Rev. X.

[12] "Nfc/rfid planar spiral coil inductance calculator." Web.

[13] S. Marley, "Measuring Inductance with an Oscilloscope and Signal Generator." Web, April 2020.

[14] Wikipedia contributors, "Lc circuit — Wikipedia, the free encyclopedia," 2021. [Online; accessed 2-April-2022].

[15] C.-S. Wang, G. Covic, and O. Stielau, "Power transfer capability and bifurcation phenomena of loosely coupled inductive power transfer systems," *IEEE Transactions on Industrial Electronics*, vol. 51, no. 1, pp. 148–157, 2004.

[16] Texas Instruments, *LM3478 High-Efficiency Low-Side N-Channel Controller for Switching Regulator*, 2017. Rev. X.